Advances in Water Resources 127 (2019) 291–309

Contents lists available at ScienceDirect

Advances in Water Resources

journal homepage: www.elsevier.com/locate/advwatres

A regularization strategy for modeling mixed-sediment river morphodynamics

Víctor Chavarrías[a,*], Guglielmo Stecca[b], Annunziato Siviglia[c], Astrid Blom[a]

[a] Faculty of Civil Engineering and Geosciences, Delft University of Technology, Delft, The Netherlands
[b] National Institute of Water and Atmospheric Research (NIWA), Christchurch, New Zealand
[c] Laboratory of Hydraulics, Hydrology and Glaciology, Swiss Federal Institute of Technology (ETH), Zurich, Switzerland

A B S T R A C T

A notable drawback in mixed-size sediment morphodynamic modeling is the fact that the most commonly used mathematical model in this field (i.e., the active layer model Hirano, 1971) can be ill-posed under certain circumstances. Under these conditions the model loses its predictive capabilities, as negligible perturbations in the initial or boundary conditions produce significant differences in the solution. In this paper we propose a preconditioning method that regularizes the model to recover well-posedness by altering the time scale of the sediment mixing processes. We compare results of the regularized model to data from four new laboratory experiments conducted under conditions in which the active layer model is ill-posed. The regularized active layer model captures the change of bed elevation and surface texture averaged over the passage of several bedforms. Neither the active layer model nor the regularized one account for small scale changes due to individual bedforms.

1. Introduction

The presence of mixed-size sediment is a key feature of rivers. Sediment sorting patterns develop in the streamwise direction (e.g., the characteristic downstream fining profile Sternberg, 1875), in the transverse direction (e.g., bend sorting Allen, 1970), and in the vertical direction (e.g., bed armoring Parker and Klingeman, 1982 and dune sorting Blom et al., 2003). Modeling applications in which the mixed-size character of river morphodynamics is not negligible mandate the use of a suitable continuity model accounting for mass conservation of each of the considered sediment size fractions. Hirano (1971) was the first to develop a mixed-sediment continuity model. He assumed that the river bed can be vertically divided into an active top part (the active layer), which interacts with the flow, and an inactive substrate. In the model, sediment transport and friction depend on the texture of the active layer, whereas the sediment in the substrate only plays a role if net aggradation creates new substrate sediment or net degradation leads to the entrainment of substrate sediment into the active layer.

Although it has been fruitfully used to represent physical phenomena related to mixed-sediment for nearly half a century (see Chavarrías et al., 2018), the active layer model suffers from a drawback. Under certain conditions it becomes ill-posed (Chavarrías et al., 2018; Ribberink, 1987; Stecca et al., 2014). A model is ill-posed if a unique solution does not exist, or if the solution does not depend continuously on the initial and boundary conditions (Hadamard, 1923). If a model is ill-posed, infinitesimal variations in the initial or boundary conditions yield a significant deviation of the solution within an infinitesimal time (Hadamard, 1923). When solving the mathematical model by numerical approximations, perturbations in the initial and boundary conditions simply arise by truncation errors. This makes an ill-posed model unsuitable in practice.

The problem of ill-posedness arises from an inaccurate representation of the physical processes (Joseph and Saut, 1990). For instance, a two-fluid model for incompressible and inviscid flow in two layers with a velocity discontinuity is ill-posed (von Helmholtz, 1868; Kelvin, 1871). It is regularized (i.e., becomes well-posed) if viscous effects are taken into account (Joseph and Saut, 1990). From this perspective, the preferred approach to regularize the active layer model would be the development of a new model that includes those physical mechanisms that are not accounted for by the active layer model.

There exist alternatives to the active layer that typically aim to improve the physical description of sediment mixing process. Ribberink (1987) introduced a second layer to account for the mixing due to dunes exceptionally larger than the average dune height. Besides producing a vertical sorting profile that better reproduces the results of a laboratory experiment (Blom, 2008), Ribberink's two-layer model makes the occurrence of ill-posedness less likely, although it does not completely avoid it (Sieben, 1994). Luu et al. (2006, 2004) proposed a model in which the active layer is replaced by the sediment transport layer representing the sediment in transport rather than the sediment at the bed surface. The thickness of the sediment transport layer is estimated with a closure relation such as the one developed by Egashira and Ashida (1992). Although conceptually different, the model by

* Corresponding author.
E-mail address: v.chavarriasborras@tudelft.nl (V. Chavarrías).

https://doi.org/10.1016/j.advwatres.2019.04.001
Received 12 June 2018; Received in revised form 20 February 2019; Accepted 2 April 2019
Available online 5 April 2019

Luu et al. (2006, 2004) is mathematically equivalent to the active layer model, which implies that it can also be ill-posed.

Blom and Parker (2004) and Blom et al. (2006, 2008) developed a model in which both bed elevation and bed grain size distribution are treated using a vertically continuous formulation (Parker et al., 2000). This implies that there is no distinction between the active and inactive part of the bed. The model by Blom and coauthors satisfactorily describes the vertical stratigraphy due to dunes at laboratory scale, but it requires a time step too small to be applicable at large scale. Moreover, its well-posedness has not been studied. Simplifying the continuous framework proposed by Parker et al. (2000), the vertically continuous model by Viparelli et al. (2017) overcomes the need for a small time step. Although applicable at large spatial and temporal scales, their model does not solve the problem of ill-posedness (Chavarrías et al., 2018).

Given the facts that: (a) There is not yet a practically feasible alternative to the active layer model, (b) the active layer model remains well-posed over a large range of applications (Chavarrías et al., 2018), and (c) it is a computationally cheap model implemented in several software packages, here our objective is to develop a strategy to avoid ill-posedness while maintaining the conceptual framework of the active layer model. To this end, we develop a regularization strategy that recovers well-posedness of the active layer model and we conduct 4 laboratory experiments under conditions in which the active layer model is ill-posed to obtain data to which we compare the results of our regularized model.

The paper is organized as follows. In Section 2 we review strategies for regularizing ill-posed models. In Section 3 we present the regularization strategy. Section 4 presents the laboratory experiments and Section 5 focuses on the numerical runs to reproduce the experimental results. In Section 6 we discuss the limitations of the regularization strategy, as well as other possible modeling strategies.

2. Overview of regularization techniques

In this section we review techniques used to regularize ill-posed problems. Propagation problems are most completely mathematically represented by a set of partial differential equations constituting an initial value problem. In these problems an initial state changes with time subject to conditions at the boundaries of the domain. The matrix-vector formulation provides a compact expression of the set of equations (e.g., Courant and Hilbert, 1989; Lyn and Goodwin, 1987; Toro, 2001):

$$\frac{\partial \mathbf{Q}}{\partial t} + \mathbf{A}\frac{\partial \mathbf{Q}}{\partial x} = \mathbf{S}, \tag{1}$$

where $\mathbf{Q}$ is the vector of dependent variables, $\mathbf{A}$ is the system matrix, and $\mathbf{S}$ is the vector of source terms. The velocity at which small waves propagate throughout the domain (i.e., the eigenvalues of matrix $\mathbf{A}$) must be real for the problem to be well-posed (e.g., Hadamard, 1923; Ivrii and Petkov, 1974; Kabanikhin, 2008; Lax, 1957; 1958; 1980; Mizohata, 1961). When the eigenvalues are real, the problem is hyperbolic. If the eigenvalues have an imaginary component (the problem being elliptic or of mixed-type), an initial value problem is ill-posed.

The two-fluid shallow flow model (i.e., a model of the flow of two layers of superimposed fluids at different velocities) is known to be ill-posed when the difference in flow velocity between the upper and lower layers exceeds a certain threshold (Ardron, 1980; Armi, 1986; Lawrence, 1990; Long, 1956; Pelanti et al., 2008). In general terms ill-posedness arises in multiphase models (e.g., bubbles in a fluid) (Harlow and Amsden, 1975; Kumbaro and Ndjinga, 2011; Murray, 1965; Stewart, 1979; Stewart and Wendroff, 1984). Multiphase models are regularized by accounting for the forces at the interface between the two fluids (Abgrall and Karni, 2009; Drew et al., 1979; Liska et al., 1995; Lyczkowski et al., 1978; Ramshaw and Trapp, 1978; Stewart, 1979; Stuhmiller, 1977; Tiselj and Petelin, 1997; Travis et al., 1976). Although the physics of multiphase problems is better represented when including the effects of the interface forces, this approach does not completely eliminate the possibility of the problem being ill-posed.

Fernández Nieto (2003), Castro Díaz et al. (2011), and Sarno et al. (2017) introduce an additional term in the momentum equations to account for friction between the fluid layers. Their regularization strategy yields a well-posed model and has a physical origin. However, the additional physical term depends on the time step of the numerical solution, which implies that it cannot be considered a fully physically-based solution.

The numerical solution of a mathematically ill-posed model can be well-posed (Chen and Peng, 2006; Chen et al., 2007; Savary and Zech, 2007; Spinewine et al., 2011) if the numerical solution neglects information in the physical equations (Greco et al., 2008). Worded differently, in such a case the physical equations are ill-posed, but the numerical equations that we actually solve are well-posed. In particular, when using the HLL solver (a common approximate Riemann solver proposed by Harten et al., 1983, see Toro, 2009), one only uses the fastest and slowest eigenvalues of the system, which implies that the dynamics due to the intermediate celerities are not resolved. This hides the problem of ill-posedness rather than solves it.

In determining the steady (equilibrium) state of a fluid dynamics problem, a commonly adopted strategy to achieve fast convergence is to modify the celerities at which information propagates (i.e., the system eigenvalues) (Chorin, 1967; Grabowski and Berger, 1976; Plows, 1968; Soh and Berger, 1984). For instance, in aerodynamics, the speed of sound may differ significantly from the air velocity, which causes a slow convergence to steady state (Choi and Merkle, 1993; Feng and Merkle, 1990; Godfrey et al., 1993; van Leer et al., 1991). Preconditioning methods (Turkel, 1987; 1993; 1999) aim at bringing the eigenvalues of the system closer to each other such that a larger time step is allowed.

Analogously, the “bed celerity” (i.e., the speed of the wave related to changes in bed elevation (Lyn and Altinakar, 2002; Morris and Williams, 1996; Stecca et al., 2014; De Vries, 1965)) is generally slow compared to the celerities associated with perturbations of the flow. This fact has encouraged the use of a “morphodynamic acceleration factor” in morphodynamic modeling to reduce the computational time (Latteux, 1995; Lesser et al., 2004; Ranasinghe et al., 2011; Roelvink, 2006). Mathematically, as we will show later, the use of a morphodynamic acceleration factor is equivalent to the application of a particular preconditioning method.

By altering the celerity at which information propagates, the transient state of the preconditioned problem is altered with respect to the original problem, but both problems converge to the same steady state solution if the boundary conditions are steady. A drawback of preconditioning is the fact that, when the problem is subject to unsteady boundary conditions, preconditioning methods modify the steady state, as they indirectly modify the timing of the boundary conditions (Turkel, 1999). For this reason, the boundary conditions of a preconditioned model need to be adjusted if these vary with time.

The fact that a preconditioning method alters the transient state was used by Zanotti et al. (2007) to regularize the two-fluid model. They modified the system of equations by introducing two parameters. One parameter modifies the continuity equation, which affects the imaginary part of the eigenvalues. Depending on the relations between velocities and densities of the two fluids, a specific value of this parameter makes the imaginary part equal to zero. Apart from modifying the imaginary component, the parameter also modifies the real part of the eigenvalues. They introduce a second parameter that affects all equations to recover the original real part of the eigenvalues. They compare the solution of the regularized model to analytical solutions and they show that the regularized two-fluid model is stable. In the next section we will follow a similar approach to derive a regularization strategy for the active layer model.

3. Regularization strategy for the active layer model

In this section we propose a strategy for recovering the well-posed character of the system of equations for modeling mixed-sediment river morphodynamics. The modified set of equations is presented in Section 3.1. In Section 3.2 - we derive the parameters used to recover the well-posed character of the model considering a simplified case with two sediment size fractions and steady flow, which allows us to obtain analytical expressions. We then extend the validity to unsteady flow conditions (Section 3.3) and to conditions with more than 2 sediment size fractions (Section 3.4). In Section 3.5 we discuss the implementation of the strategy.

3.1. Modified system of equations

We consider one-dimensional hydrostatic flow over a bed composed of N non-cohesive size fractions. The flow is described by the Saint-Venant (1871) equations. We assume a Chézy-type friction in which the nondimensional friction coefficient is independent of the flow and bed parameters. The sediment transport rate is considered to adapt instantaneously to changes in the bed shear stress (Bell and Sutherland, 1983). The mass conservation of the bed sediment is described by the Exner (1920) equation, and the $N-1$ active layer equations (Hirano, 1971) account for the conservation of the mass of each grain size fraction within a discrete top layer of the bed surface (i.e., the active layer). Given the flow, friction, and sediment transport assumptions, the model cannot represent small-scale processes (i.e., processes at the scale of bed elevation fluctuations due the stochastic nature of sediment transport, ripples, dunes, or bed load sheets). In other words, the variables represent parameters averaged over a period larger than the characteristic time of small-scale bed elevation fluctuations (Armanini and di Silvio, 1988; Blom et al., 2008; Parker et al., 2000; Ribberink, 1987; Wong and Parker, 2006). We refer to Appendix A for the model equations and the matrix-vector formulation of the system.

Analogous to Zanotti et al. (2007) (Section 2), the system of equations in Equation (1) is modified multiplying the time derivative term by a diagonal matrix $\mathbf{M}$ to regularize the problem:

$$\mathbf{M}\frac{\partial \mathbf{Q}}{\partial t}+\mathbf{A}\frac{\partial \mathbf{Q}}{\partial x}=\mathbf{S}. \tag{2}$$

Matrix $\mathbf{M}$ modifies the transient state only. The preconditioning technique does not affect the solution of the steady state (i.e., $\partial/\partial t = 0$).

The morphodynamic model under unisize conditions was analyzed by Cordier et al. (2011). They found that the Saint-Venant-Exner model is always well-posed assuming a Chézy-type friction. This confirms that the ill-posed character of the mixed-size sediment model results from the inappropriate representation of the mixing processes by the active layer model (Chavarrías et al., 2018). For this reason, we propose a regularization strategy that recovers the well-posed character modifying the celerities at which mixed sediment processes occur. This is done by means of a set of parameters α_k [−] for $1 \le k \le N-1$ that multiply the time derivative of each active layer equation. Similarly to Zanotti et al. (2007), we consider a parameter β [−] that can be used to rescale the celerities after being modified by α_k. We stipulate that this parameter β affects only the sediment processes (including the Exner (1920) equation) but not the flow.

The modified system of equations must be mass conservative with respect to the sediment. This implies that α_k cannot be grain size dependent (i.e., $\alpha_k = \alpha\ \forall k$) and that the preconditioning technique is only applicable when the active layer thickness is constant (Appendix B).

3.2. Derivation of the regularization coefficients

In this section we derive the values of the coefficients α and β that enable regularization of the active layer model. We consider a simplified case with two sediment size fractions under steady flow conditions, as this allows us to obtain analytical expressions of the regularization parameters.

In this case, the dependent variables of the system are the bed elevation η [m] and the volume of fine sediment in the active layer per unit of bed area, M_{a1} [−] (Chavarrías et al., 2018 and Appendix A):

$$\mathbf{Q}_{s2}=\left[\eta, M_{a1}\right]^{\intercal}. \tag{3}$$

The system matrix is:

$$\mathbf{A}_{s2}=u\begin{bmatrix}\lambda_b & \dfrac{\lambda_{s1}}{\mu_{1,1}}\\ \lambda_b\gamma_1 & \lambda_{s1}\end{bmatrix}, \tag{4}$$

where the parameters λ_b [−] and λ_{s1} [−] are the nondimensional approximated bed and sorting celerities, which (approximately) represent the celerities at which infinitesimal perturbations in bed level and grain size distribution of the bed surface propagate through the domain (Chavarrías et al., 2018; Stecca et al., 2014; De Vries, 1965 and Appendix A.5), and u [m/s] is the mean flow velocity. The parameters γ_1 [−] and $\mu_{1,1}$ [−] relate the changes in the sediment transport rate to the properties of the bed (Appendix A.5). Subscript s indicates that the model is steady and subscript 2 highlights that it accounts for two sediment size fractions only.

The preconditioning matrix is:

$$\mathbf{M}_{s2}=\beta\begin{bmatrix}1 & 0\\ 0 & \alpha\end{bmatrix}. \tag{5}$$

Note that β does not affect the mathematical character of the system, as it modifies all equations equally. Worded differently, the parameter β changes the magnitude of the eigenvalues but not the type (real or complex). We compute the eigenvalues (λ_k for $k = 1, 2$) of the modified system of equations as the roots of the characteristic polynomial $\det(\mathbf{M}_{s2}\lambda - \mathbf{A}_{s2}) = 0$:

$$\lambda_k=\frac{u}{2\beta}\left(\lambda_b+\frac{\lambda_{s1}}{\alpha}\pm\frac{\sqrt{\Delta}}{\alpha}\right)\quad\text{for}\quad k=1,2, \tag{6}$$

where the discriminant Δ is a second degree polynomial on α equal to:

$$\Delta=\lambda_b^2\alpha^2+2\lambda_b\lambda_{s1}\left(\frac{2\gamma_1}{\mu_{1,1}}-1\right)\alpha+\lambda_{s1}^2. \tag{7}$$

We consider a situation which is ill-posed if the regularization strategy is not applied. This implies that when $\alpha = 1$ (the regularization strategy is not applied), $\Delta < 0$ (the eigenvalues are complex). We aim to modify the system of equations as little as possible in regularizing it. Worded differently, we aim at changing α as little as possible from 1. The minimum modification is obtained when the discriminant is equal to 0 (i.e., the eigenvalues are in the limit for having an imaginary part different than 0). The threshold values α_c that modify the system of equations as little as possible are found by equating (7) to zero:

$$\alpha_c=\frac{\lambda_{s1}}{\lambda_b}\left(1-2\frac{\gamma_1}{\mu_{1,1}}\pm2\sqrt{\frac{\gamma_1}{\mu_{1,1}}\left(\frac{\gamma_1}{\mu_{1,1}}-1\right)}\right). \tag{8}$$

There are two possible values of α_c that yield real eigenvalues. The discriminant (Eq. (7)) as a function of α is a concave parabola as $\lambda_b^2 > 0$. Moreover, when $\alpha = 0$, $\Delta = \lambda_{s1}^2 > 0$ and when $\alpha = 1$, $\Delta < 0$. This shows that one critical value of parameter α is between 0 and 1, and the second value is larger than 1 (i.e., $0 < \alpha_{c1} < 1 < \alpha_{c2}$).

We compute the value of parameter β that, assuming $\alpha = \alpha_c$, recovers the real part that the eigenvalues would have if they had not been modified using the parameter α:

$$\beta=\frac{\lambda_b+\lambda_{s1}/\alpha_c}{\lambda_b+\lambda_{s1}}. \tag{9}$$

In this case, irrespective of the value of α, the eigenvalues of the regularized system are equal to:

$$\lambda_k=\frac{u}{2}\left(\lambda_b+\lambda_{s1}\right)\quad\text{for}\quad k=1,2. \tag{10}$$

If we do not use β to recover the original real part of the eigenvalues (i.e., if $\beta = 1$), the eigenvalues of the regularized system are equal to

$$\lambda_k = \frac{u}{2}\left(\lambda_b + \frac{\lambda_{s1}}{\alpha}\right) \quad \text{for} \quad k = 1, 2. \tag{11}$$

Parameter α can be selected to be larger or smaller than 1 and if we choose to use β (i.e., if $\beta \neq 1$) the eigenvalues are independent of α. Summarizing, we find three possible regularization strategies:

1. $\alpha \neq 1$ and $\beta \neq 1$
2. $\alpha < 1$ and $\beta = 1$
3. $\alpha > 1$ and $\beta = 1$

In general terms, the approximated sorting celerities are positive, and under subcritical flow conditions (i.e, Fr < 1) the approximated bed celerity is also positive. However, due to hiding in the sediment transport relation, under conditions in which ill-posedness likely occurs, λ_{s1} may be negative regardless of the Froude number (Chavarrías et al., 2018). In this case, Strategies 1 and 2 do not guarantee that the eigenvalues $\lambda_k > 0$. We consider that it is physically unrealistic that morphodynamic information travels in the upstream direction under subcritical flow conditions. A negative eigenvalue would imply that the boundary condition for morphology needs to be imposed at the downstream end to yield a well-posed model, and this is contradictory to the fact that the morphodynamic state under subcritical flow conditions depends on the load coming from upstream (Blom et al., 2017a; 2016). On the other hand, Strategy 3 guarantees that $\lambda_k > 0$ (Appendix A of the supplementary material). Thus, we consider that the only possible regularization strategy is the one in which $\alpha > 1$ and $\beta = 1$.

We need to guarantee that the celerities of the system of equations modified by the regularization strategy are not physically unrealistic. In particular, under a sufficiently small Froude number, the modified bed and sorting celerities must be significantly smaller than the celerities of the flow. The regularization technique does not modify the approximated celerity associated with bed elevation changes (i.e., $\beta = 1$) and decreases the celerity associated with mixing processes (i.e., $\alpha > 1$, we will discuss this point in Section 6.1). For this reason, the regularization technique does not cause the celerities to be physically unrealistic.

The regularization strategy is not limited to a particular range of parameter settings. Yet, when using the value of α derived in this section, the Froude number cannot be in the transcritical region, as in this case the quasi-steady approximation is not valid (Cao and Carling, 2002b; Cao et al., 2002; Colombini and Stocchino, 2005; Lyn, 1987; Lyn and Altinakar, 2002; Sieben, 1999). In the following section we consider unsteady flow, which extends the regularization technique to the transcritical region.

3.3. Validity under unsteady flow conditions

In this section we extend the validity of the regularization parameter α found for steady flow cases (Section 3.2) to unsteady flow conditions.

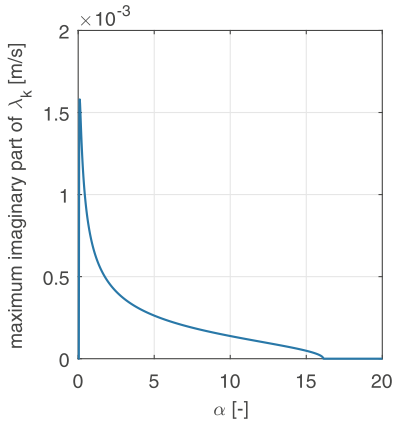

Fig. 1. Maximum imaginary part of all the eigenvalues of the reference case (Table 1) as a function of α. In this case $\alpha_c = 16.1$ is the smallest value of $\alpha > 1$ that yields a well-posed model (i.e., all eigenvalues are real).

Table 1
Reference values in the comparison of the value of α_c computed analytically and numerically.

u [m/s]	h [m]	C_f [–]	L_a [m]	F_{a1} [–]	f_l^1 [–]	d_1 [m]	d_2 [m]
1	1	0.01	0.20	0	1	0.001	0.005

When considering unsteady flow conditions, we cannot obtain an analytical expression of α_c for regularizing the system of equations. Nevertheless we can numerically find the smallest value of $\alpha > 1$ for which the roots of the characteristic polynomial of $\det(\mathbf{M}_u\lambda - \mathbf{A}_u) = 0$ are real values (i.e., the eigenvalues are real), where subscript u indicates that the model is unsteady. Matrices $\mathbf{M}_u$ and $\mathbf{A}_u$ are listed in Appendix A.5. This procedure is nonetheless expensive computationally in comparison with an algebraic calculation. Fig. 1 shows the maximum imaginary part of all eigenvalues of a reference ill-posed case (Table 1) considering unsteady flow for varying α. The sediment transport rate is computed using a fractional version of the Engelund and Hansen (1967) sediment transport relation (Blom et al., 2017a). A value $\alpha > 16.1$ yields a well-posed model (i.e., all eigenvalues are real).

To test the validity of the algebraic value of α_c obtained assuming steady flow we consider the same reference case (Table 1) and we vary the flow velocity to obtain a range of conditions. In Fig. 2(a) we present the value of α_c necessary to obtain a well-posed model computed assuming steady flow (Eq. (8)) and numerically considering unsteady flow. We conclude that for a Froude number below approximately 0.6, there is no significant difference between the values for steady and unsteady flow. This implies that, for Fr < 0.6, the value of α_c obtained analytically assuming steady flow is a good approximation of the actual value.

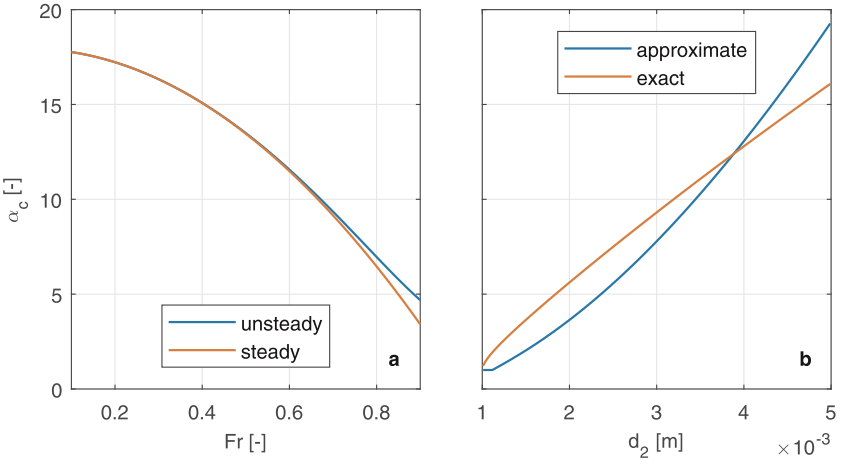

Fig. 2. Comparison between (**a**) the steady and unsteady values of the regularization parameter α_c, and (**b**) the exact and approximate values for a 3 size fractions case.

3.4. Validity under multiple size fractions conditions

In a model with more than 2 size fractions, we cannot analytically obtain the value of α_c that regularizes the active layer model. Similar to the unsteady case, it is possible to numerically obtain the smallest value of $\alpha > 1$ that yields real eigenvalues computed as the roots of the characteristic polynomial $\det(\mathbf{M}_s\lambda - \mathbf{A}_s) = 0$ (matrices $\mathbf{M}_s$ and $\mathbf{A}_s$ are presented in Appendix A.5). Again, this process is relatively expensive in computational terms. In this section we propose a method to obtain an approximate value of α_c for such cases and compare it to the exact value obtained numerically.

Assuming steady flow, a system that models N sediment size fractions has N equations (Appendix A). We reduce the system of N equations to an approximate system of 2 equations following the approach of Ribberink (1987). We sum the N active layer equations to obtain one equation that models the changes of the mean grain size of the bed surface sediment (Appendix A.3). Subsequently, we apply the same technique as the one we have used in the case of 2 size fractions to obtain a critical value of α that guarantees that the approximate model is well-posed:

$$\alpha_{cm} = \frac{\lambda_m}{\lambda_b}\left(1 - 2\frac{\gamma_m}{\mu_m} \pm 2\sqrt{\frac{\gamma_m}{\mu_m}\left(\frac{\gamma_m}{\mu_m} - 1\right)}\right), \tag{12}$$

where the symbols are the equivalent of the case for two size fractions in the approximate model (Appendix A.5)

We consider a case with 3 sediment size fractions, where the fine and coarse fractions have characteristic sizes equal to $d_1 = 0.001$ m and $d_3 = 0.005$ m, respectively. The volume fraction contents of the 3 size fractions in the active layer are $F_{a1} = 0$, $F_{a2} = 0.9$, and $F_{a3} = 0.1$. The substrate is fully composed of fine sediment. We vary the medium grain size (d_2) to obtain a range of conditions. The remaining parameters are the same as the ones presented in Table 1. In Fig. 2(b) we compare the exact value of α_c (computed numerically) to the approximated one (computed using Eq. (12)). The approximated value of α_c follows the same trend as the exact one. However, the approximated value is both larger and smaller than the exact one depending on the sediment conditions. This implies that the current approximate approach may be insufficient to regularize the active layer model in the case of more than 2 sediment size fractions.

The approximate system of equations can be ill-posed under degradational conditions into a fine substrate only (Chavarrías et al., 2018; Ribberink, 1987). However, a 3 size fractions case can be ill-posed under degradational conditions into a coarse substrate (Chavarrías et al., 2018), which further limits the applicability of the approximate solution for the threshold value of α.

3.5. Implementation

In this section we describe our approach for numerically solving the system of equations and apply the regularization strategy.

We have developed the numerical research code Elv to model mixed-size sediment river morphodynamics (Blom et al., 2017a; 2017b) which solves the equations for flow, bed elevation, and the bed surface grain size distribution in a decoupled manner (i.e., in series and not as a coupled system of equations). Thus, our code is not appropriate for solving transcritical situations (Lyn, 1987; Lyn and Altinakar, 2002; Sieben, 1999) or cases with a high sediment concentration (Cao and Carling, 2002a; Morris and Williams, 1996).

The one-dimensional spatial domain is discretized using an equispaced grid. All variables are computed at the cell centers and are considered constant in each time step. Here we assume steady flow, which is represented by the backwater equation (Eq. (16)). This ordinary differential equation is integrated using the standard fourth-order finite difference Runge–Kutta method (RK4). The Exner (1920) equation (Eq. (17)) and active layer equation (Eq. (19)) are solved in conservative form using a first order upwind scheme in combination with forward Euler to integrate in time. We discretize the vertical domain in a finite number of cells having a certain thickness to account for stratigraphic changes in the substrate. Our scheme is balanced for the vertical fluxes between the active layer and the substrate (Stecca et al., 2016). This means that mass conservation is guaranteed independent of the substrate discretization. The time step varies with time and is computed such that the CFL number (Courant et al., 1928) is constant and equal to 0.9 (Toro, 2009; Wu, 2007). The details of the numerical implementation are described in Appendix B of the supplementary material.

When the regularization strategy is applied, we first determine the mathematical character of the model (i.e., well-posed or ill-posed) at each node using the approach proposed by Chavarrías et al. (2018). For the case of 2 size fractions, this is done evaluating an algebraic equation, and for more than 2 size fractions we numerically compute the eigenvalues of the system matrix. At continuation, for each node we compute the threshold value α_c that guarantees that the model is well-posed. Again, this is done evaluating an algebraic expression (Eq. (8)) for 2 size fractions and it is done numerically for more than 2 size fractions (Section 3.4).

The regularization strategy yields equal eigenvalues (i.e., in a two size fractions case $\lambda_1 = \lambda_2$, Eq. (11)). This implies that the problem is hyperbolic but not strictly hyperbolic (Cordier et al., 2011; Lax, 1980; Toro, 2009). In a non-strictly hyperbolic problem, the solution may not be unique and resonance may occur, which gives rise to strong non-linear interactions (Isaacson and Temple, 1992; Liu, 1987). In avoiding a non-strictly hyperbolic-problem, we modify the value of α_c using a small parameter $\epsilon > 0$ [−] such that $\alpha^* = \alpha_c(1 + \epsilon)$, where α^* [−] is the value used for updating the bed surface grain size distribution. For the cases we have studied a value of $\epsilon = 0.005$ is sufficient to avoid the problems associated with non-strict hyperbolicity.

Ill-posedness causes short-wave instability (Chavarrías et al., 2018; Joseph and Saut, 1990 and Section 5.1.2) meaning that perturbations will grow unstable at rates depending on the inverse of their length. Diffusion counteracts these effects by dampening perturbations (Gray and Ancey, 2011). Regularization of the problem can be provided by numerical diffusion if a first-order (diffusive) method is used. However, if the underlying problem is ill-posed, cell refinement will be able to reveal its ill-posed character even if a first-order method is used in its solution, as we do in this paper. This is because, with decreasing cell size, the numerical diffusion coefficient of a first-order method will generally decrease, while at the same time shorter (more unstable) perturbations will be solved. Therefore, an ill-posed problem will show no convergence due to its inherent instability when the mesh is progressively refined, regardless of the low-order method in use.

We observe such a behavior in Section 5.1.2 where we show that our low-order numerical scheme suffices to capture the consequences of ill-posedness by revealing instability and non-converging character in simulations conducted within the ill-posed range. It is likely that, with a higher-order (non-diffusive) method, these features would have become apparent even at lower mesh resolution due to absence of spurious diffusion dampening perturbations. However, it must be considered that our upwind scheme is characterized by small numerical diffusion coefficient, and that Stecca et al. (2016) and Siviglia et al. (2017) have shown that a first-order upwind scheme with a fine grid resolution is sufficient to capture the main features of mixed-size sediment morphodynamic simulations such as the ones we conduct.

4. Laboratory experiments

In this section we describe the laboratory experiments conducted under conditions in which the active layer model (Hirano, 1971) is ill-posed in order to obtain a data set to which we can compare the results of the proposed regularization strategy. We describe the experimental plan, materials, and measurements in Section 4.1. In Section 4.2 we present the experimental results.

4.1. Experimental plan and measurements

We conducted 4 laboratory experiments (I1, I2, I3, and I4). The experiments reproduced degradational conditions into a fine substrate, which are conditions prone to be ill-posed (Chavarrías et al., 2018; Ribberink, 1987; Stecca et al., 2014). The experiments were conducted in a 14 m long, 0.40 m wide, and 0.45 m high tilting flume in the Water Laboratory of the Faculty of Civil Engineering and Geosciences of Delft University of Technology. At the upstream end, a turbulence dissipation device was installed (item (a) in Fig. 3). An inclined plane was placed downstream from the turbulence dissipation device (item (b) in Fig. 3) to allow for an alluvial bed (item (c) in Fig. 3). The structure was covered with glued sediment such that friction was similar to the one of the alluvial bed. Its elevation could be adjusted.

We consider a reference system with coordinate origin at the bottom of the flume at the downstream end of the metal structure. The z-axis is parallel to gravity and pointing up. The x-axis follows the streamwise direction of the flume, being positive in the direction of the flow. The y-axis is perpendicular to the other two axes forming a right handed orthonormal basis.

We used two sediment size fractions (fine and coarse) with characteristic grain sizes (computed as the arithmetic mean in ϕ scale) equal to 2.1 mm and 5.5 mm. The standard deviation of the two size fractions is 1.1 mm and 1.2 mm, respectively. The bed surface was initially flat, with a constant slope, and composed of coarse sediment only. Below a 0.03 m thick layer of coarse sediment, we installed a patch of fine sediment of varying length L_p [m] (Fig. 3 and Table 2). We imposed a constant water discharge and a constant sediment feed rate of the coarse fraction only, which was in equilibrium with the initial condition (Table 3 and Appendix C of the supplementary material). The sediment was introduced using a feeder placed on top of the flume (item (d) in Fig. 3). The downstream water level was lowered at a rate of 0.01 m/h during 8 h by adjusting a sharp-crested weir at $x = 12.60$ m (item (g) in Fig. 3). The lowering of the water level led to bed degradation and entrainment of the fine sediment in the patch. We have tested that in these conditions the active layer model is ill-posed regardless of the active layer thickness and sediment transport relation.

Sediment was collected in a sand trap (item (e) in Fig. 3) at the downstream end of the flume ($x = 12.10$ m). The sediment was pumped from the sand trap (item (f) in Fig. 3) into a tank positioned on a weight balance next to the flume. This system allowed us to continuously measure the sediment transport rate. The water inflow was measured using an ultrasonic flow meter and the downstream water level using a position sensor. We obtained profiles of the water and bed elevation using laser sensors that were fixed to a carriage (item (h) in Fig. 3). A camera was mounted on the carriage to measure the grain size distribution of the bed surface using the technique developed by Orrú et al. (2016a,b) (item (i) in Fig. 3). To this end, the coarse sediment was painted red and the fine sediment blue. Our experimental set-up allowed us to measure either a profile of bed and water surface elevation or the bed surface grain size distribution at a certain location with time.

For the modeling of the laboratory experiments (Section 5), it is important to obtain turbulent flow conditions of a relatively deep flow (i.e., flow cannot be affected by individual grains), where sediment is predominantly transported as bed load. The concentration of sediment needs to be so small that we can assume clear water. These conditions were satisfied (Appendix C of the supplementary material).

Table 2
Length (L_p) and position (initial x_{p0} and final x_{pf} coordinates) of the patch of fine sediment below the coarse bed surface.

Experiment	L_p [m]	x_{p0} [m]	x_{pf} [m]
I1	0.50	4.70	5.20
I2	1.00	4.49	5.49
I3	2.00	4.47	6.47
I4	4.00	4.47	8.47

Table 3
Experimental conditions, where q denotes water discharge per unit width, s_0 initial bed slope, q_{b0} sediment feed rate per unit width, h flow depth, u mean flow velocity, and Fr is the Froude number.

q [m^2/s]	s_0 [–]	q_{b0} [m^2/s]	h [m]	u [m/s]	Fr [–]
0.150	3.50×10^{-3}	7.86×10^{-6}	0.187	0.799	0.59

4.2. Results

All experiments were governed by the same conditions before the fine sediment in the patch was entrained. We observed the superposition of bedforms of two different length scales (Fig. 4). Secondary bedforms approximately 0.5 m long and 0.01 m high were superimposed on primary longer bedforms of the order of 3 m and twice as high. The primary

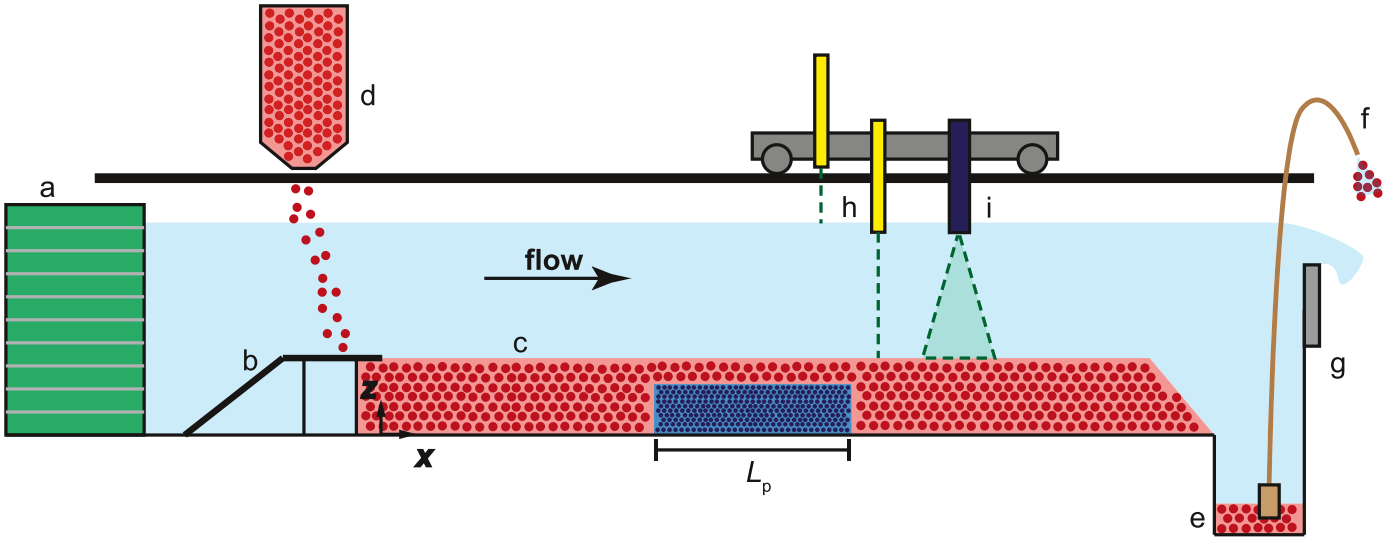

Fig. 3. Sketch of the flume set-up: (**a**) Turbulence dissipator, (**b**) metal plate with glued sediment, (**c**) alluvial bed, (**d**) feeder, (**e**) sand trap, (**f**) sediment pump, (**g**) weir, (**h**) laser sensors for water and bed surface elevation, and (**i**) camera for measuring the bed surface grain size distribution.

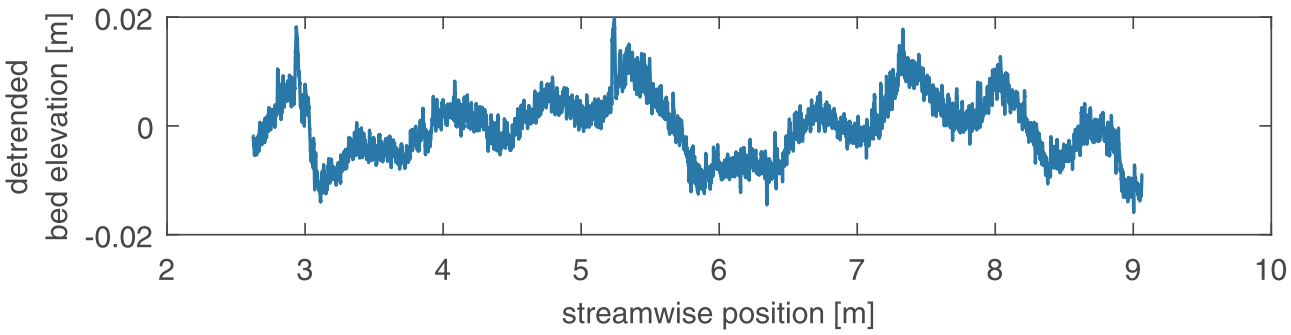

Fig. 4. Measured bed elevation before fine sediment of the patches is entrained showing the superposition of bedforms of two different length scales (Experiment I4 at 1:51 h).

bedforms are interpreted as incipient gravel dunes (Carling, 1999; Carling et al., 2005). The characteristics of these features remained steady as the bed degraded. The steadiness of the features' characteristics is confirmed in a preparatory experimental run without a patch of fine sediment (Appendix C of the supplementary material).

After approximately 2 h the bed had degraded up to a point at which the trough of a long bedform was lower than the top part of the patch (Fig. 5(a)). At that moment fine sediment was exposed, entrained, and transported. The larger mobility of the fine sediment created a downstream moving degradational wave (Fig. 5(b)). As erosion proceeded, the shear stress was reduced (due to the increased flow depth), which reduced the degradation rate. Meanwhile, the subsequent bedform advanced and started to fill the degradational pit with coarse sediment (Fig. 5(c)). Overall, the passage of bedforms induced entrainment of fine sediment and subsequent coarsening of the top part of the substrate. Since the degradational wave increased in depth in downstream direction, also the thickness of the coarse top layer increased in downstream direction (Fig. 5(d)).

The substrate coarsening mechanism created an irregular interface between coarse and fine sediment compared to the initial situation where the interface was parallel to the bed surface. As a consequence, the entrainment of fine sediment became a pseudo-random process in space and time. Degradational waves formed at those locations where fine sediment was closest to the bed surface. Yet, most of the waves grew for only a limited length, as, due to the irregular interface, at some point the sediment present at the trough was coarse rather than fine. Sometimes the interface was sufficiently parallel to the bed surface and a large degradational wave formed. This is seen in the content of coarse sediment at the bed surface of the patch (Fig. 6(a), (c), (e) and (g)) and in the bed elevation (Fig. 7). One or two small degradational waves formed after the passage of a large degradational wave, characterized by the fact that the bed surface is composed of mainly fine sediment and the trough of a bedform reaches elevations significantly lower than average.

A longer patch allowed for the development of longer (in space and time) and deeper erosional waves (Figs. 6 and 7). Yet, the decrease in degradation rate as the wave advanced acted as a saturation mechanism limiting the height of the wave. Thus, the probability of lower bed elevation at the patch zone was not significantly larger for an increasing patch length (Fig. 8). After the patch, where the substrate was composed of coarse sediment only, wave height decreased and the bed elevation profile tended to the one upstream of the patch (Fig. 7). Yet, the presence of fine sediment downstream of the patch slightly increased the height of the bedforms with respect to the bedforms upstream of the patch (Fig. 8(a) and (c)). Bedforms downstream of the patch were characterized by a coarse front and fine tail, and were approximately 2 grain sizes of the coarse sediment high. These characteristics may indicate the presence of bedload sheets (Dietrich et al., 1989; Recking et al., 2009; Whiting et al., 1988) or bedforms in a transitional phase to small dunes. The domain downstream from the patch was not long enough to precisely conclude on the type of bedforms. The changes in volume fraction content of coarse sediment at the bed surface were less pronounced downstream of the patch compared to at the patch (Fig. 6(b), (d), (f) and (h)). This is because fine sediment entrained at the patch dispersed in the downstream direction.

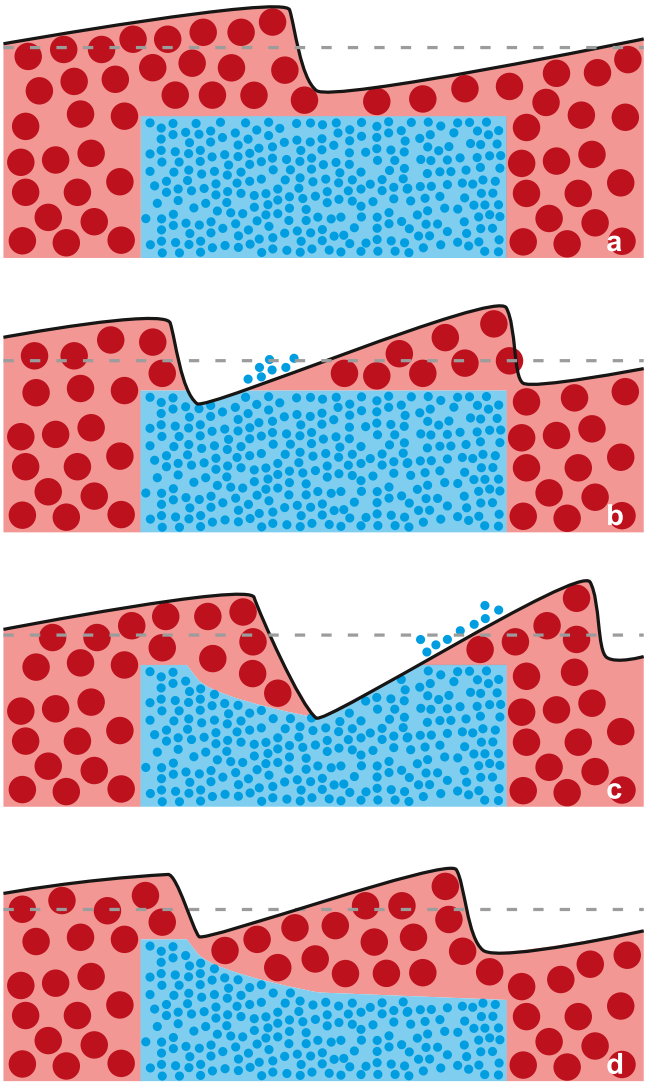

Fig. 5. Sketch of the cyclic entrainment of substrate sediment: (**a**) Bedforms formed out of coarse sediments only, (**b**) fine sediment from the patch is entrained in the trough of a bedform, (**c**) a degradational wave forms and travels downstream, (**d**) coarse sediment from upstream fills the pit left by the degradational wave.

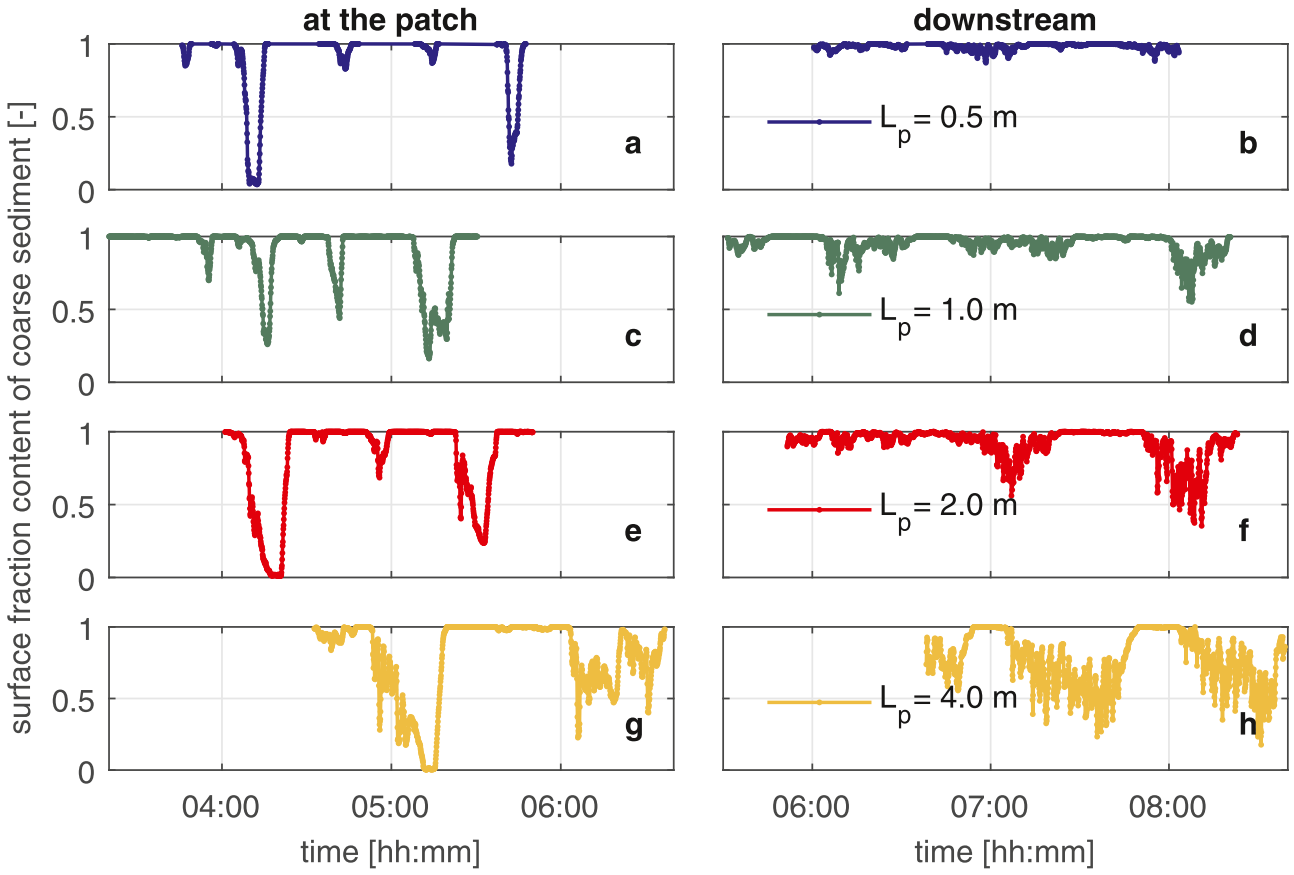

Fig. 6. Measured surface fraction content of coarse sediment as a function of time for various lengths of the patch L_p: At the center of the patch (**a,c,e,g**), and at the downstream end (**b,d,f,h**). Note that the streamwise location of the center of the patch varies for each experiment while the downstream position is the same for all cases ($x = 9.15$ m).

5. Numerical modeling

In this section we apply the regularization strategy in modeling the laboratory experiments conducted under conditions in which the active layer model is ill-posed (Section 5.1). In Section 5.2 we compare the results of the regularized active layer model to the results of the two-layer model developed by Ribberink (1987) by applying them to a thought experiment under conditions in which the active layer model is ill-posed.

5.1. Modeling of our laboratory experiments

In Section 5.1.1 we calibrate the numerical model. In Section 5.1.2 we conduct a convergence test to show the consequences of ill-posedness and the benefits of the regularization strategy. In Section 5.1.3 we apply the numerical model to the laboratory experiments described in the previous section. In Section 5.1.4 we test the regularization strategy assuming three sediment size fractions.

5.1.1. Calibration

Modeling the laboratory experiments requires values for the active layer thickness and the friction coefficient, and the choice of a sediment transport relation. To this end we use the results of a set of preparatory experiments (Appendix C of the supplementary material). To chose a sediment transport relation, we run two experiments conducted under equilibrium conditions, while feeding the fine and the coarse sediment size fractions. The sediment transport relation by Ashida and Michiue (1971) reproduces our results reasonably well (Appendix D of the supplementary material). To obtain the skin friction coefficient (C_{fb}) for computing the sediment transport rate (Appendix A.4) we correct the total measured friction coefficient C_f for side wall friction with the method developed by Johnson (1942) (see Guo, 2015). We obtain the values $C_f = 0.0104$ and $C_{fb} = 0.0084$. Bedform drag was negligible during the initial phase as bedforms were low. When fine sediment was entrained, bedforms grew and bedform drag may have played a role. It is not reasonable to model this additional friction using standard relations (e.g. Engelund and Hansen, 1967; Haque and Mahmood, 1983; Wright and Parker, 2004), as these relations provide a bedform-averaged friction coefficient, while in our case large bedforms were isolated in space and time. We decide to use a constant friction coefficient and we think that the most sensible approach is to neglect bedform drag.

A reasonable value for the active layer thickness is 0.01 m, which corresponds to the distance below the mean bed elevation with a probability of entrainment below approximately 5% (Blom, 2008; Ribberink, 1987). This value is also in accordance with 1–3 times D_{90} as proposed by, for instance, Hirano (1971); Hoey and Ferguson (1994), and Seminara et al. (1996).

In one preparatory experiment under equilibrium conditions, we fed coarse sediment only and, from some point, we started feeding tracer sediment (i.e., sediment of a different color). Modeling the propagation of the front of tracer sediment, we confirm that 0.01 m is a reasonable value for the active layer thickness (Appendix D of the supplementary material).

5.1.2. Convergence test

First we aim to show the consequences of ill-posedness. To this end, we simulate conditions similar to the ones of the experiments using the active layer model. In the experiments, degradation into a coarse substrate (i.e., under well-posed conditions) occurred for approximately 2 h, as the patch of fine sediment was placed 3 cm below the initial bed surface. In order to obtain ill-posed conditions at

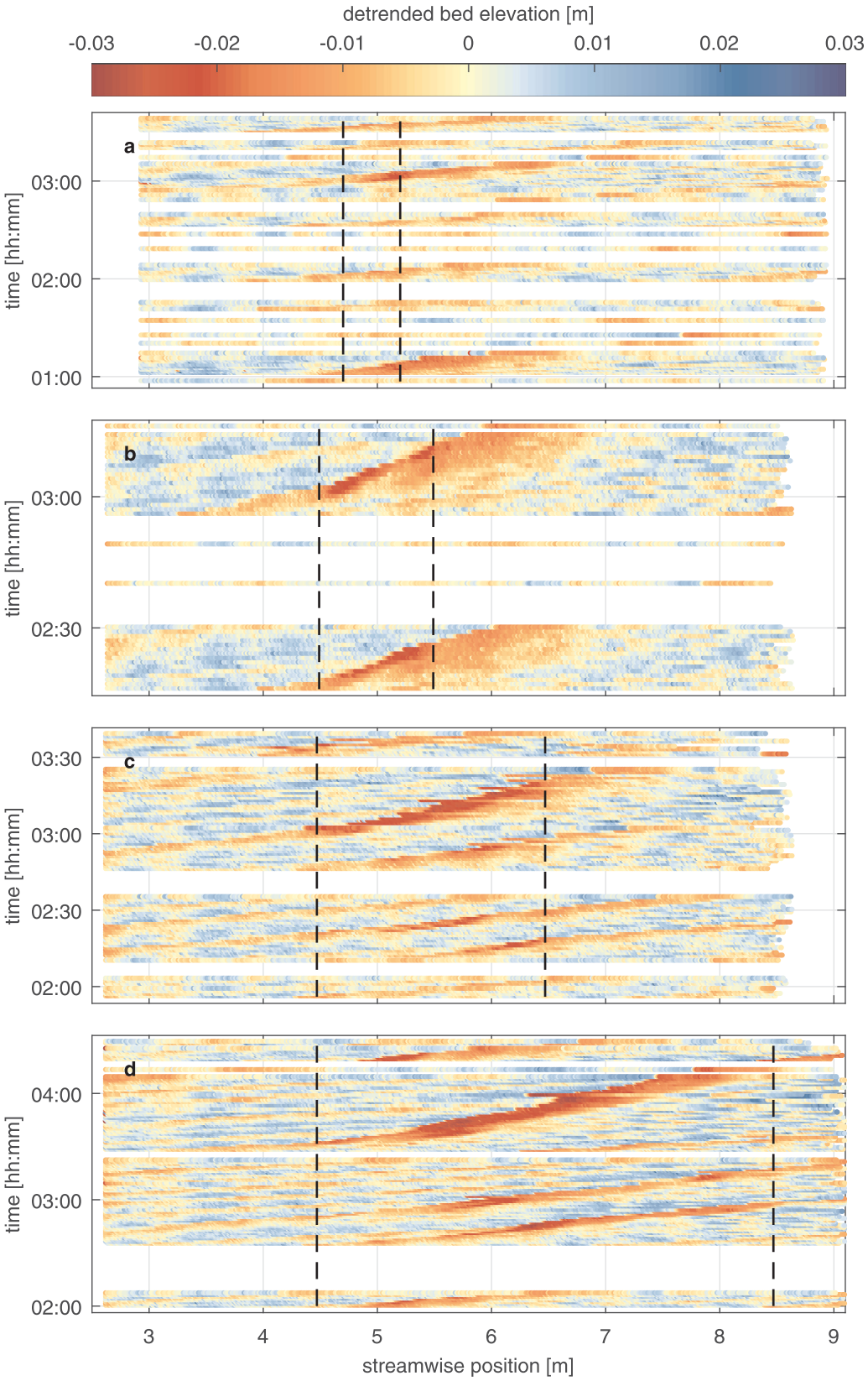

Fig. 7. Detrended bed elevation as a function of time in Experiment (**a**) I1, (**b**) I2, (**c**) I3, and (**d**) I4. The dashed black lines indicate the boundaries of the patch. The bed elevation is detrended subtracting the bed slope of each profile individually, obtained fitting a first degree polynomial.

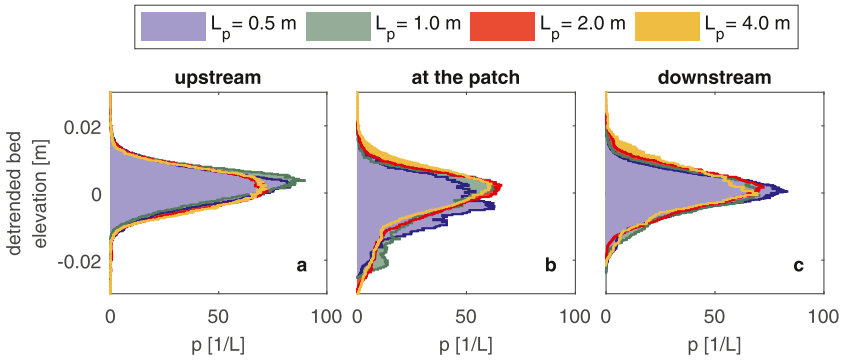

Fig. 8. Probability density of detrended bed elevation: (**a**) Upstream of the patch, (**b**) at the patch, (**c**) and downstream of the patch.

the start of the simulations, the patch of fine sediment is placed right below the active layer. In this manner, 300 s simulations suffice for our purpose. Moreover, the patch extends over a distance of 8 m (from $x = 1$ m to $x = 9$ m) to maximize the domain over which the model is ill-posed.

We conduct 13 simulations using cell sizes ranging from 0.1 m down to 2.44×10^{-5} m. The results do not converge and continue to change as the grid is refined (Fig. 9(a)). We compute the error as a function of the cell size to quantify the (lack of) convergence. As there is no analytical solution to which we can compare the results of the numerical runs,

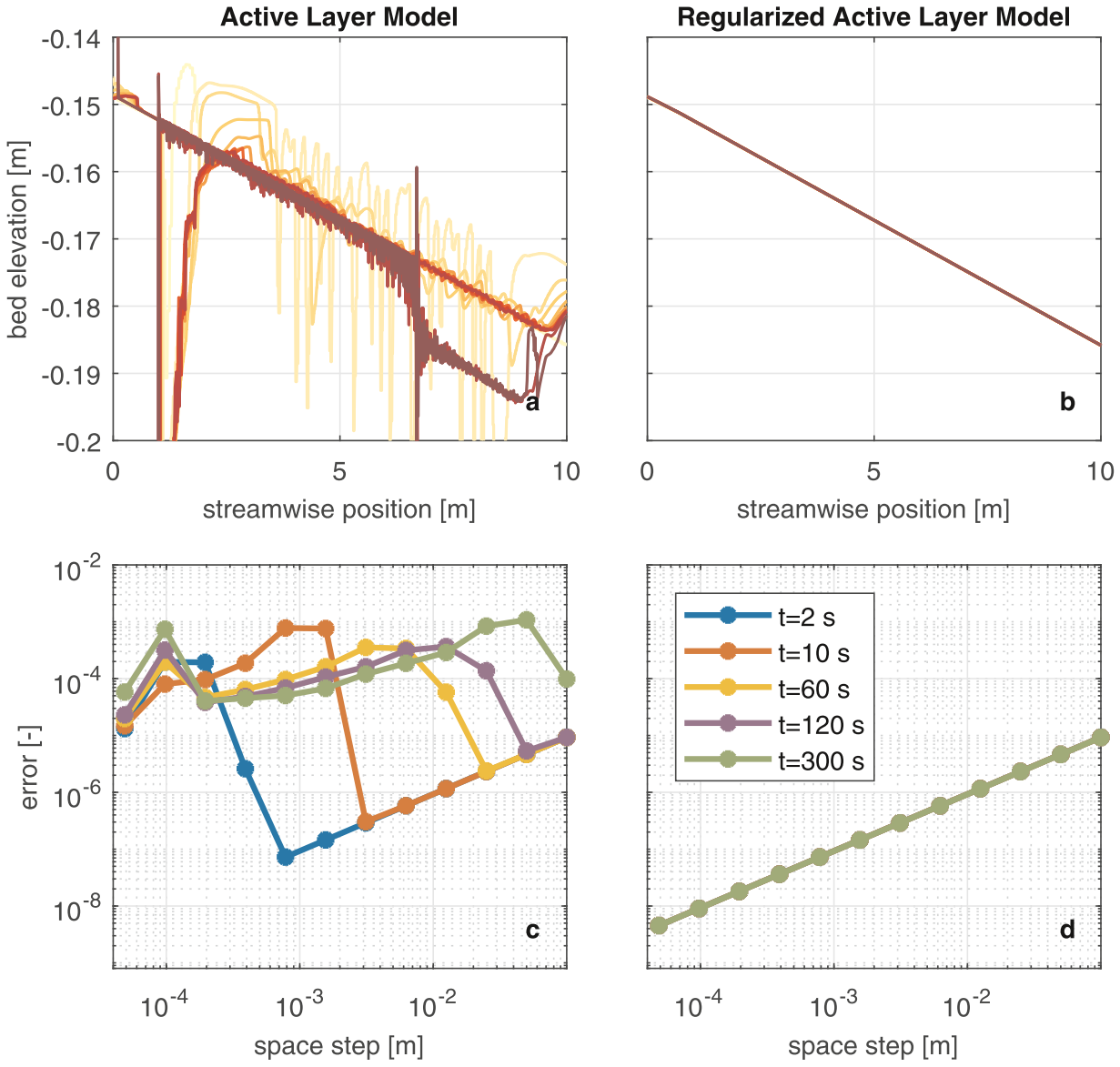

Fig. 9. Bed elevation at $t = 300$ s predicted using the (**a**) active layer model (Hirano, 1971) and (**b**) regularized active layer model. Each of the 13 lines presents the results computed using a different cell size (ranging from 0.1 m down to 2.44×10^{-5} m, where darker colors represent smaller cell sizes). Panels (**c**) and (**d**) present the error at a certain time using a particular cell size (see Equation (13)) when using the active layer model and the regularized active layer model, respectively. In panels (**b**) and (**d**) only one line is visible, as it overlaps all other lines.

we compute the error between the results of two successive simulations s and $s+1$ (Love and Rider, 2013; Roy, 2005). To this end, first we interpolate the bed elevation results of all simulations using the smallest cell size. The interpolation, rather than linear, takes into consideration that each value is constant inside a cell. Second, we compute the error as the norm 1 of the difference between bed elevations of two successive simulations at a certain time t:

$$\text{error}_s^t = \frac{1}{LN_x}\sum_{r=1}^{N_x}\left|\eta_{r_s}^t - \eta_{r_{s+1}}^t\right|, \tag{13}$$

where N_x denotes the number of cells of the simulation with the smallest cell size, and L [m] the domain length. Fig. 9(c) shows the error as a function of the cell size for several times. If the cell size is large (for instance, larger than 0.01 m), for short simulation times (for instance, shorten than 10 s), the results seem to converge. Yet, using the same cell size, the results do not converge if one considers a longer simulation time. Similarly, considering a simulation time equal to 10 s, the results do not converge when the cell size is smaller than 0.002 m. This behavior is characteristic of ill-posed simulations. The growth rate of perturbations increases with decreasing cell size. For this reason, the consequences of ill-posedness arise earlier for smaller cell sizes. Given a certain cell size, if the simulation is short enough, perturbations do not have time to grow and the solution seems to converge. For a fixed time, simulations seem to converge after the error grows (for instance, for $t = 120$ s, simulations seem to converge for cell sizes between 0.001 m and 0.01 m). This is due to the fact that, at the given time, perturbations have already grown significantly and have coarsened the bed material causing the simulation to be well-posed. A further decrease of the cell size or an analysis at a different time shows that the active layer model does not converge.

We repeat the same simulations applying the regularization strategy. The initial value of the parameter that recovers the well-posed character of the system is $\alpha_c = 11.6$. In this case the solution does not show oscillations (Fig. 9(b)). Moreover, the solution converges for a decreasing cell size independently from the time at which convergence is tested (Fig. 9(d)). This supports the fact that the regularized model is well-posed, contrary to the active layer model. The rate at which the solution converges confirms that the numerical scheme is first-order accurate (Section 3.5).

5.1.3. Two sediment size fractions

We reproduce all laboratory experiments using a cell size equal to 0.05 m. The regularized model shows spatial or temporal oscillations in none of the cases (Fig. 10). For all cases the bed elevation decreases smoothly in the streamwise direction (Fig. 10(b), (f), (j) and (n)). This contrasts with the measured temporal change of bed elevation, which presents bedforms and the formation of degradational waves at the upstream end of the patch (Fig. 10(a), (e), (i) and (m)). The measured increase in wave height at the patch (Fig. 10(a), (e), (i) and (m)) and Section 4.2) is not captured. The effect of the patch is observed in the model results in the fact that degradation occurs faster for a long patch (Fig. 10) than for a short one (Fig. 10(b)).

The continuous and smooth predicted entrainment of substrate sediment yields an almost steady volume fraction content of sediment in the active layer both at the patch (Fig. 10(c), (g), (k) and (o)) and at the downstream end (Fig. 10(d), (h), (l) and (p)). The measured data shows, on the other hand, a variable volume fraction content at the bed surface. The model correctly captures the mean value and nicely reproduces that a longer patch causes an increase in the amount of fine sediment at the bed surface. The fact that the model does not capture bedforms is not surprising, as the mechanisms necessary for bedform formation are not present in the model. For instance, the fact that the flow model is based on the hydrostatic pressure assumption prevents modelling processes such as flow separation. The possibility of capturing the formation of the degradational waves at the patch is also discarded, as from the analysis of well-posedness we see that the regularized model does not show any instability mechanism that could induce wave growth. For this reason, the model results represent values averaged over the passage of several bedforms and degradational waves. We choose not to filter the measured bed elevation data, as given the characteristics of the bedforms, it would introduce a large amount of spurious information (e.g., the degradational wave would start at the wrong location) and we would lose a significant amount of data at the beginning and end of the domain.

Overall the regularized model yields a reasonable approximation of the mean temporal change of the measured data. The degradational trend is captured and the surface grain size distribution approximates the average measured values. The substrate is not unrealistically altered as there are no oscillations in the solution.

5.1.4. Three sediment size fractions

To test the regularization strategy for multiple grain sizes, we model Experiment I4 (Table 2) using 3 different grain sizes by applying the exact solution to obtain the regularization parameter. The fine size fraction remains the same and the previous coarse size fraction is represented in this case by two characteristic grain sizes equal to 4.895 mm and 5.895 mm. For an initial volume fraction content at the bed surface of the medium size sediment equal to 0.375, the initial bed slope is the same as when using two characteristic sizes and the sum of the sediment transport rate of the medium and coarse fractions when using three sizes is equal to the sediment transport rate of the coarse fraction when using two sizes. In this manner the simulation accounting for three sediment fractions is comparable to the one accounting for two size fractions.

In Fig. 11 we compare the bed elevation and mean grain size of the bed surface sediment predicted by the regularized model using 2 and 3 sediment size fractions. The evolution of the bed elevation shows only a weak dependence on the number of size fractions used to discretize the sediment mixture. The model with 3 size fractions presents a mild coarsening (0.2% increase in mean grain size) with time before sediment from the patch is entrained (after 2 h). This coarsening is not visible when using 2 size fractions, because in this case, during the initial state, the bed surface sediment consists of one single grain size only. We conclude that the regularization technique is applicable for a general case with more than 2 size fractions.

5.2. Comparison between Ribberink's (1987) two-layer model and the regularized model

To our knowledge there is no other laboratory data set apart from the one presented in Section 4 to which we can apply the regularized active layer model to test its performance. This is because either the conditions that other researchers have studied yield a well-posed active layer model (e.g. Ashida and Michiue, 1971) or the active layer model is ill-posed but the active layer thickness varies with time due to dune growth (Blom et al., 2003). The latter case is a situation that the regularization strategy cannot deal with (Section 3.1). However, Ribberink (1987) applies his two-layer model to a thought experiment under conditions in which the active layer model is ill-posed. In this section we apply the regularized active layer model to his thought experiment and compare it to the two-layer model.

Ribberink (1987) conducted a laboratory experiment with mixed-size sediment, which was dominated by aggradation after a period of degradation (Experiment E8-E9). The initial bed was characterized by a uniform slope, composed of a bimodal mixture (a coarse and fine fraction), and well mixed both in the streamwise and vertical direction. The sediment supply was initially in equilibrium. A temporal increase of the proportion of the coarse fraction in the sediment supply perturbed the equilibrium condition and induced the downstream propagation of a coarsening wave. The downstream migration of the coarsening front caused a preceding and temporary bed degradation as a result of the

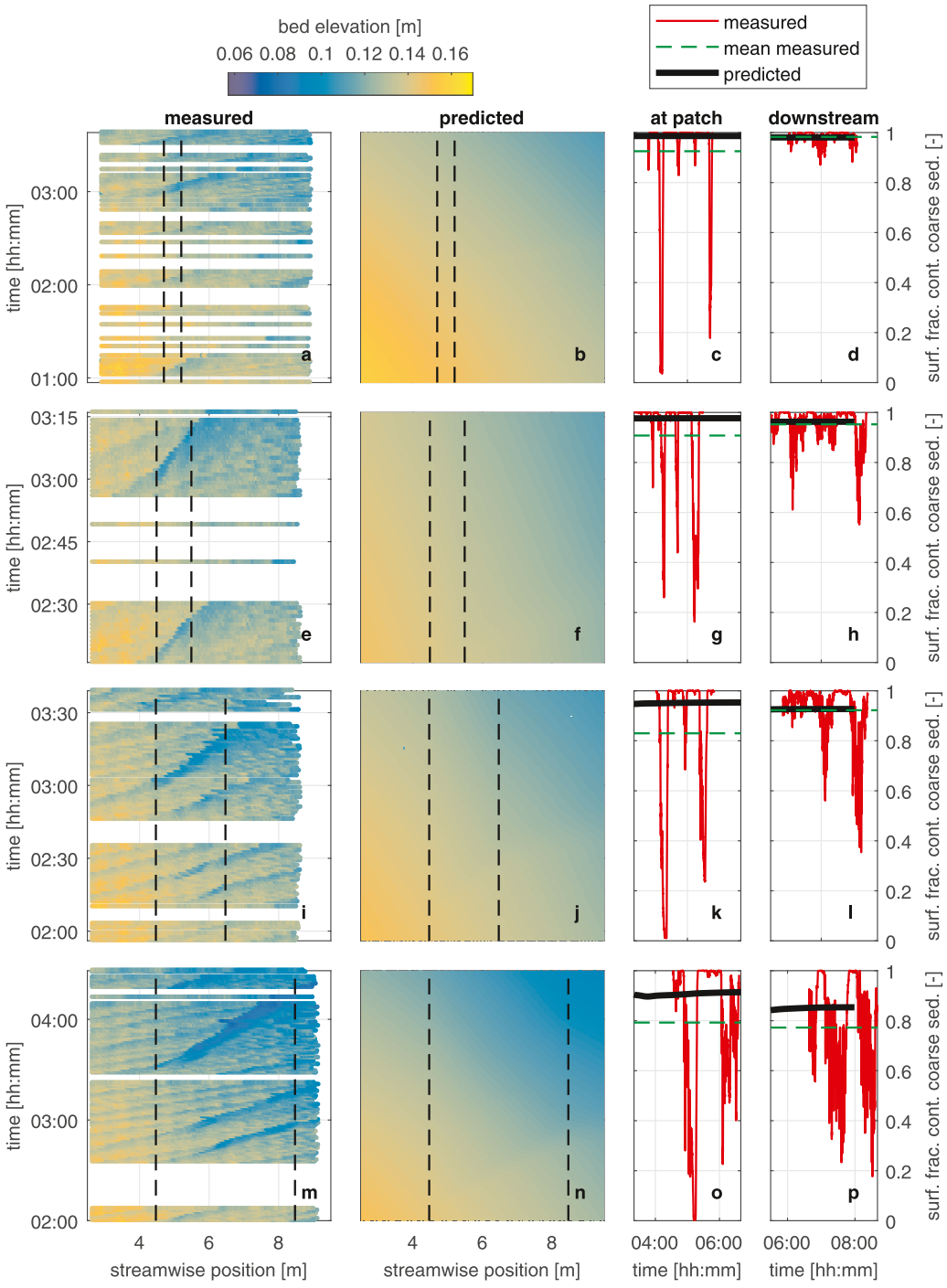

Fig. 10. Comparison between measured data and regularized model results: Experiment I1 (**a**-**d**), Experiment I2 (**e**-**h**), Experiment I3 (**i**-**l**), and Experiment I4 (**m**-**p**). The first and second columns show the measured and predicted bed elevation with time, respectively. The vertical dashed lines indicate the position of the patch of fine sediment. The third and fourth columns present the surface fraction content of coarse sediment at the center of the patch of fine sediment and at the downstream end of the flume, respectively.

difference in sediment mobility between the coarse sediment forming the wedge and the fine sediment downstream of the front of the wedge. Eventually, the bed aggraded and was characterized by a larger slope than the initial one, so as to allow for the transport of the coarser fed sediment under equilibrium conditions.

During the short degradational part of the experiment, the bed surface was coarser than the substrate (i.e., conditions in which the active layer model is prone to be ill-posed Chavarrías et al., 2018; Ribberink, 1987; Stecca et al., 2014). However, while reproducing the experiment numerically, Ribberink (1987) found that the active layer model was well-posed. Subsequently, Ribberink (1987) applied his two-layer model to a thought experiment that was equal to E8-E9 except for the fact that the substrate sediment was finer than in the flume experiment such that the active layer model is ill-posed. A numerical simulation of the thought experiment using the active layer model showed oscillations that eventually made the code crash (Ribberink, 1987). The thought experiment was reproduced well by a numerical code implementing Ribberink's (1987) two-layer model.

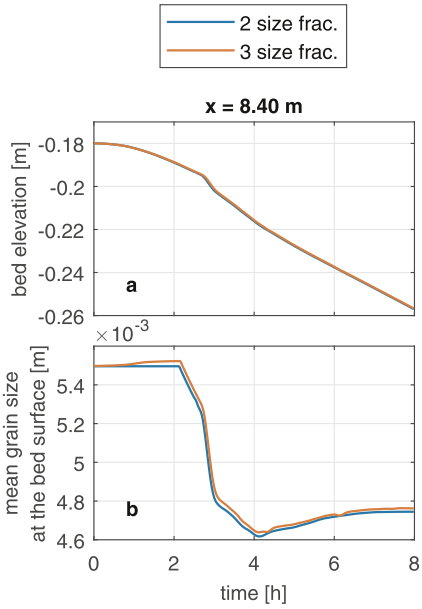

Fig. 11. Bed elevation (**a**) and mean grain size at the bed surface (**b**) as a function of time predicted in Experiment I4 using the regularized active layer model using 2 and 3 sediment sizes.

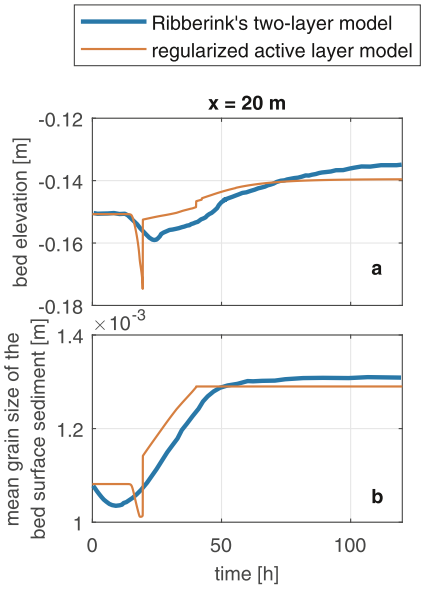

Fig. 12. Bed elevation (**a**) and mean grain size of the bed surface sediment (**b**) with time predicted for the thought experiment based on Experiment E8-E9 conducted by Ribberink (1987) using Ribberink's two-layer model and the regularized active layer model. The results of the two-layer model are extracted from Fig. 7.9 of Ribberink (1987).

Here we run a numerical simulation of the thought experiment using our regularized active layer model and compare it to the results of Ribberink's (1987) two-layer model reported in Fig. 7.9 of Ribberink (1987). Simulation details can be found in Appendix C.

Fig. 12 presents the time series of bed elevation and mean grain size of the bed surface sediment at a location 20 m downstream from the inlet. During the first 20 h the effects of the coarsening of the fed sediment are not felt 20 m downstream from the inlet. While the regularized active layer model predicts a constant bed elevation and grain size distribution of the bed surface sediment during this period of time, the two-layer model predicts a fining of the bed surface (Fig. 12(b)). This is due to the fact that the initial grain size distribution of the exchange layer is not in equilibrium with the one at the active layer and causes a vertical flux of sediment. However, the bed elevation remains constant as predicted by both models (Fig. 12(a)).

The aggradational phase is preceded by a degradational wave, which is much more pronounced in the regularized active layer model than in the two-layer model. This is because in the regularized active layer model degradation causes entrainment of the fine substrate sediment, whereas in the two-layer model the exchange layer acts as a buffer that slows down the process. The coarsening of the bed surface between approximately 25 h and 40 h as predicted by both models is very similar. While after 40 h the regularized active layer model predicts a constant grain size distribution of the bed surface sediment, the two-layer model predicts an asymptotic adaptation toward equilibrium conditions. This effect is again caused by the exchange layer that coarsens slowly compared to the active layer on top of it, as it accounts for the effects of occasionally large bedforms. The equilibrium state differs between the two models. We believe that this is due to the fact that we do not know exactly what values were used by Ribberink (1987) for the constants in the sediment transport relation (Appendix C).

The regularized active layer model captures the dynamics predicted by the two-layer model of Ribberink (1987). The advantage of the two-layer model is that it accounts for a source of vertical mixing that the regularized active layer model does not take into consideration (i.e., the mixing due to occasionally large bedforms). On the other hand, the two-layer model may become ill-posed (Sieben, 1994) while the regularized active layer model is always well-posed.

6. Discussion

In this section we discuss the physical interpretation of the regularization strategy (Section 6.1), as well as possible extensions and further development (Section 6.2).

6.1. Physical interpretation of the regularization strategy

The ill-posed solution predicted by the active layer model is characterized by oscillations that temporarily fine the bed surface and coarsen the substrate. This behavior is also observed in our laboratory experiments (Figs. 6 and 7). One may be tempted to conclude that the active layer model, although being mathematically ill-posed, provides reasonable results. This argument is wrong for two reasons. The first reason is that the numerical solution does not converge for a decreasing mesh size. The solution keeps changing and oscillations become larger when the cell size is reduced (Chavarrías et al., 2018; Joseph and Saut, 1990). Such a solution cannot be representative of physical phenomena. Second, the physical processes responsible for the small scale variability in bed elevation (i.e., ripples, bedload sheets) are not accounted for by the active layer model (Section 3.1). Any resemblance of the model results with bed elevation fluctuations due to small scale bedforms is therefore coincidence.

The frequently used morphodynamic factor (Φ_η) (Latteux, 1995; Ranasinghe et al., 2011; Roelvink, 2006) is a particular case of a preconditioning matrix with parameters $\beta = 1/\Phi_\eta$ and $\alpha_k = 1\ \forall k$. The proposed regularization strategy can be considered as the use of a morphodynamic factor not only for the changes in bed elevation (η) but also for the changes in grain size distribution of the bed surface (M_{ak}). The "sorting morphodynamic factor" (Φ_{sk}) is then defined as $\Phi_{sk} = 1/(\alpha_k \beta)$. We have seen that the only applicable regularization strategy is that in which $\alpha_k = \alpha > 1\ \forall k$ and $\beta = 1$, which is equivalent to saying that the regularization strategy is based on a "sorting morphodynamic factor" $0 < \Phi_s < 1$. This implies that the mixing or sorting processes associated with changes in grain size distribution of the bed surface sediment are slowed down with respect to the celerity predicted by the active layer model.

The effect of applying the regularization strategy is a slowdown of the sediment mixing processes in the model computations. This effect is similar to the effect of a (temporary) increase of the active layer thickness. From a physical perspective this slowdown of mixing processes may be associated with a (temporary) increase of the range of elevations covered by the bed level fluctuations (Blom et al., 2008). The slowdown of mixing processes resulting from applying the regularization strategy implies that the regularized active layer model can be applied to a wider range of physical problems (i.e., also those characterized by a fairly small time scale of mixing) than the active layer model.

6.2. Alternatives to the regularization strategy

Our regularization strategy is applied locally and temporally. Worded differently, only when and where the model is ill-posed, we update the grain size distribution of the bed surface sediment using the parameter α_c. Moreover, α_c depends only on the conditions at the location under consideration (note that the preconditioning matrix is diagonal). This is the simplest strategy but one could decide to avoid discontinuities in the value of α_c throughout the domain by coupling neighboring nodes.

Carraro et al. (2018) propose a technique to decrease the computational cost of morphodynamic simulations. As in our case, their strategy can be seen as a preconditioning technique. They consider unisize sediment conditions and modify not only the Exner (1920) equation but also the continuity equation. Here we modify the active layer equation but not the flow equations or the Exner (1920) equation. A combination of both strategies could yield a technique that both decreases the cost of numerical simulations and guarantees that the model is well-posed.

We have focused on restoring the hyperbolic character of the system of equations and to this end we based our study on the linear solution (i.e., short waves). This focus suffices here, as short waves are most sensitive to ill-posedness (Joseph and Saut, 1990). However, the regularization strategy modifies the celerity and growth rate not only of short waves but also of long ones. For this reason, we suggest to further study how long waves are affected and whether the results of the regularization strategy are physically realistic based on a similar analysis to that of Lanzoni et al. (2006).

We have assumed a constant active layer thickness to avoid the added complexity due to a cumbersome closure relation linking the preconditioning parameters to the change in time of the active layer thickness. It may be possible to extend our regularization strategy to situations in which the active layer thickness changes with time (e.g., due to dune growth) by providing such a closure relation. On the other hand, it is reasonable that the regularization strategy requires a constant active layer thickness given the fact that mathematically the strategy has the same effect as an increase in the active layer thickness (i.e., a decrease in the celerity of the mixing processes).

We have concluded that the regularization strategy needs to slowdown the mixing processes (i.e., $\alpha_c > 1$) to guarantee that the eigenvalues are always positive regardless of the value of the sorting celerity λ_{s1}. However, if the sorting celerity is guaranteed to be positive (e.g., because hiding is negligible), the acceleration of the mixing processes also yields positive eigenvalues and a well-posed model. There may be cases in which the latter strategy yields more realistic results. Moreover, we have chosen to guarantee that the regularized eigenvalues are positive reasoning that morphodynamic information travels in the downstream direction under subcritical conditions (Lanzoni et al., 2006; Lyn and Altinakar, 2002; Stecca et al., 2014; Suzuki, 1976). This statement is partially contradictory to recent studies that consider sediment transport as a stochastic process (Ancey and Heyman, 2014; Furbish et al., 2012). The stochastic nature of sediment transport yields an advection-diffusion equation that models the amount of moving particles per unit of bed area. The diffusive character implies that information also travels in the upstream direction. For this reason, a regularization strategy in which information travels in the upstream direction may be physically realistic under certain circumstances.

For a case with more than two sediment size fractions (Section 3.4), the approximate value of the parameter α_c is not (completely) satisfactory as well-posedness is not guaranteed. We have observed in our tests that ill-posedness occurs when (at least) two eigenvalues of the bed and sorting eigenvalues are similar with respect to the other bed and sorting eigenvalues. For a case considering two sediment size fractions this is referred in literature as the “crossing of eigenvalues” (Sieben, 1997; Stecca et al., 2014). Worded differently, the difference between two eigenvalues must be large enough for the model to be well-posed. A regularization strategy based on guaranteeing a minimum distance between eigenvalues could yield an inexpensive solution for the case with more than two sediment size fractions.

7. Conclusions

We have developed a preconditioning method for regularizing the active layer model (Hirano, 1971) used in modeling mixed-sediment river morphodynamics. Our method recovers the well-posed character of the system of equations by means of one parameter that modifies the celerity of the mixing processes. Physically this means that the mixing processes are slowed down or the time scale of the mixing processes is increased.

We conduct 4 laboratory experiments under conditions in which the active layer model is ill-posed and we compare the observations to the predictions of the regularized active layer model. The regularized active layer model captures the mean behavior observed in the experiments associated with changes averaged over the passage of several bedforms.

Acknowledgments

This research is part of the research programme RiverCare, supported by the Dutch Applied and Engineering Sciences (AES) domain of the Netherlands Organization for Scientific Research (NWO), and which is partly funded by the Ministry of Economic Affairs under grant number P12-14 (Perspective Programme). The involvement of Guglielmo Stecca was supported by NIWA under the Sustainable Water Allocation Programme. The fruitful discussions and comments on the manuscript of Liselot Arkesteijn are gratefully acknowledged. We thank the Editor Prof. Dr. G.C. Sander, Associate Editor Dr. C. Manes, and three anonymous reviewers for their comments, which have significantly improved the manuscript.

Appendix A. Model equations

In this section we present the system of equations for modeling mixed-sediment river morphodynamics. In Section A.1 we present the flow equations. In Section A.2 we present the active layer model (Hirano, 1971). A simplified active layer model is presented in Section A.3. In Section A.4 we show the closure relations. In Section A.5 we present the system of equations in matrix-vector formulation.

A.1. Flow equations

We consider a one-dimensional mixture of water and sediment flowing over a mobile bed. A set of partial differential equations that accounts for the interactions between sediment and water is found by applying mass and momentum conservation principles for the mixture of sediment and water (e.g., Garegnani et al., 2011; Greco et al., 2012). The complete system of equations reduces to the Saint–Venant–Exner model (i.e., clear water approximation) under low sediment concentrations ($c = q_b/q < 0.006$, where q_b [m^2/s] and q [m^2/s] are the sediment transport rate and flow discharge per unit width, respectively e.g.,

Garegnani et al., 2011; Garegnani et al., 2013). In the remaining we will assume that the clear water approximation is valid.

The flow is modeled using the Saint-Venant (1871) equations:

$$\frac{\partial h}{\partial t} + \frac{\partial q}{\partial x} = 0, \tag{14}$$

$$\frac{\partial q}{\partial t} + \frac{\partial (q^2/h + g h^2/2)}{\partial x} + g h \frac{\partial \eta}{\partial x} = -g h S_\mathrm{f}, \tag{15}$$

where t [s] denotes the time coordinate, x [m] the streamwise coordinate, h [m] the flow depth, g [m/s^2] the acceleration due to gravity, η [m] the bed elevation, and S_f [−] the friction slope.

The flow equations can be further simplified assuming steady flow. Under this condition the conservation of water mass and momentum reduce to a spatially constant discharge, and the backwater equation:

$$\frac{\partial h}{\partial x} = \frac{-1}{1-\mathrm{Fr}^2}\frac{\partial \eta}{\partial x} - \frac{S_\mathrm{f}}{1-\mathrm{Fr}^2}, \tag{16}$$

where $\mathrm{Fr} = q/\sqrt{g h^3}$ is the Froude number.

A.2. Active layer model

To model changes in bed elevation we assume that the sediment transport rate adapts instantaneously to changes in bed shear stress. Spatial and/or temporal adaptation to capacity load (Bell and Sutherland, 1983; Phillips and Sutherland, 1989; 1990) is not considered. Neglecting mechanisms such as subsidence and uplift (Paola and Voller, 2005), and assuming a constant bed porosity, we obtain the Exner (1920) equation:

$$\frac{\partial \eta}{\partial t} + \frac{\partial q_\mathrm{b}}{\partial x} = 0, \tag{17}$$

where for simplicity the sediment transport rate includes the pores.

The sediment phase is composed of a mixture of N non-cohesive sediment size fractions. Each fraction is characterized by a grain size d_k [m] where k is an index identifying a size fraction. The total sediment transport rate per unit width is the sum of the sediment transport rate of size fraction k, $q_{\mathrm{b}k}$ [m^2/s]:

$$q_\mathrm{b} = \sum_{k=1}^{N} q_{\mathrm{b}k}. \tag{18}$$

The conservation of the volume of sediment of size fraction k in the active layer per unit of bed area ($M_{ak} = F_{ak} L_\mathrm{a}$ [m]) is expressed mathematically as (Hirano, 1971):

$$\frac{\partial M_{ak}}{\partial t} + f_k^\mathrm{I}\frac{\partial (\eta - L_\mathrm{a})}{\partial t} + \frac{\partial q_{\mathrm{b}k}}{\partial x} = 0 \quad \text{for } 1 \le k \le N-1, \tag{19}$$

where $F_{ak} \in [0, 1]$ [−] is the volume fraction content of size fraction k in the active layer, $f_k^\mathrm{I} \in [0, 1]$ [−] is the volume fraction content of size fraction k at the interface between the active layer and the substrate, and L_a [m] is the active layer thickness. By definition,

$$\sum_{k=1}^{N} F_{ak} = 1, \quad \sum_{k=1}^{N} f_k^\mathrm{I} = 1. \tag{20}$$

From the first constrain in Eq. (20) one obtains the change of the volume of sediment in the active layer of the Nth grain size with time.

The system is complete with an equation for the conservation of mass in the substrate. Yet, this equation is linearly dependent on the Exner (1920) and Hirano (1971) equations which implies that it does not play a role in the mathematical character of the system (Chavarrías et al., 2018; Stecca et al., 2014).

A.3. Simplified Active Layer Model

To simplify the system of equations we replace the $N-1$ equations that account for the change in bed surface volume fraction content of the N fractions by one equation that models the average grain size following the approach of Ribberink (1987). We multiply each regularized active layer equation by its characteristic grain size and we add all the equations:

$$\alpha \frac{\partial D_\mathrm{ma}}{\partial t} - \frac{D_\mathrm{m}^\mathrm{I}}{L_\mathrm{a}}\frac{\partial q_\mathrm{b}}{\partial x} + \frac{1}{L_\mathrm{a}}\sum_{k=1}^{N} d_k \frac{\partial q_{\mathrm{b}k}}{\partial x} = 0, \tag{21}$$

where $D_\mathrm{ma} = \sum_{k=1}^{N} d_k F_{ak}$ [m] is the mean grain size of the sediment in the active layer and $D_\mathrm{m}^\mathrm{I} = \sum_{k=1}^{N} d_k f_k^\mathrm{I}$ [m] is the mean grain size of the sediment at the interface between the active layer and the substrate. The mean grain size is computed arithmetically as it is a necessary step to obtain an approximate equation. Yet, we consider that the mean grain size is better approximated assuming the grain size distribution to be logarithmically distributed.

We write the sediment transport rate $q_{\mathrm{b}k}$ as a function of the flow depth h and the mean grain size of the sediment in the active layer D_ma such that:

$$\frac{\partial q_{\mathrm{b}k}}{\partial x} = \frac{\partial q_{\mathrm{b}k}}{\partial h}\frac{\partial h}{\partial x} + \frac{\partial q_{\mathrm{b}k}}{\partial D_\mathrm{ma}}\frac{\partial D_\mathrm{ma}}{\partial x}. \tag{22}$$

We use that:

$$D_\mathrm{ma} = \sum_{k=1}^{N} d_k F_{ak} = d_N + \frac{1}{L_\mathrm{a}}\sum_{k=1}^{N-1} M_{ak}\left(d_k - d_N\right), \tag{23}$$

where we have used the constrain that $\sum_{k=1}^{N} F_{ak} = 1$. Thus,

$$\frac{\partial q_{\mathrm{b}k}}{\partial D_\mathrm{ma}} = \sum_{l=1}^{N-1}\frac{\partial q_{\mathrm{b}k}}{\partial M_{al}}\frac{\partial M_{al}}{\partial D_\mathrm{ma}} = L_\mathrm{a}\sum_{l=1}^{N-1}\frac{1}{d_l - d_N}\frac{\partial q_{\mathrm{b}k}}{\partial M_{al}}, \tag{24}$$

where we have used that:

$$\frac{\partial M_{al}}{\partial D_\mathrm{ma}} = \frac{L_\mathrm{a}}{d_l - d_N}. \tag{25}$$

We substitute the backwater equation (Eq. 16) in the Exner (1920) equation (Eq. 17) and the equation of the mean grain size (Eq. 21) to obtain the final set of equations:

$$\frac{\partial \eta}{\partial t} - \frac{1}{1-\mathrm{Fr}^2}\frac{\partial q_\mathrm{b}}{\partial h}\frac{\partial \eta}{\partial x} + \frac{\partial q_\mathrm{b}}{\partial D_\mathrm{ma}}\frac{\partial D_\mathrm{ma}}{\partial x} = \frac{1}{1-\mathrm{Fr}^2}\frac{\partial q_\mathrm{b}}{\partial h}S_\mathrm{f}, \tag{26}$$

$$\begin{aligned}
&\alpha\frac{\partial D_\mathrm{ma}}{\partial t} + \frac{1}{L_\mathrm{a}}\frac{1}{1-\mathrm{Fr}^2}\left[D_\mathrm{m}^\mathrm{I}\frac{\partial q_\mathrm{b}}{\partial h} - \sum_{k=1}^{N} d_k\frac{\partial q_{\mathrm{b}k}}{\partial h}\right]\frac{\partial \eta}{\partial x} \\
&\quad - \frac{1}{L_\mathrm{a}}\left[D_\mathrm{m}^\mathrm{I}\frac{\partial q_\mathrm{b}}{\partial D_\mathrm{ma}} - \sum_{k=1}^{N} d_k\frac{\partial q_{\mathrm{b}k}}{\partial D_\mathrm{ma}}\right]\frac{\partial D_\mathrm{ma}}{\partial x} \\
&= \frac{-1}{L_\mathrm{a}\left(1-\mathrm{Fr}^2\right)}\left[D_\mathrm{m}^\mathrm{I}\frac{\partial q_\mathrm{b}}{\partial h} - \sum_{k=1}^{N} d_k\frac{\partial q_{\mathrm{b}k}}{\partial h}\right]S_\mathrm{f}.
\end{aligned} \tag{27}$$

A.4. Closure relations

To close the system of equations we provide closure relations for the friction term, the sediment transport rate, and the flux between the active layer and the substrate.

We adopt the following Chézy closure relation for the friction term:

$$S_\mathrm{f} = \frac{C_\mathrm{f} u^2}{g h}, \tag{28}$$

where C_f [−] is a nondimensional friction coefficient that we assume to be constant (i.e., independent of the flow or bed properties), and $u = q/h$ [m/s] is the mean flow velocity.

The sediment transport rate of size fraction k per unit width is assumed to be the product of a nondimensional sediment transport rate ($q_{\mathrm{b}k}^*$ [−]) and the bed surface fraction content. The latter we assume equal to the active layer volume fraction content. The Einstein (1950) parameter ($\sqrt{g R d_k^3}$) scales the nondimensional quantity such that:

$$q_{\mathrm{b}k} = F_{ak}\sqrt{g R d_k^3}(1-p) q_{\mathrm{b}k}^*, \tag{29}$$

where $R = \rho_s/\rho_w - 1$ [−] is the submerged specific gravity, $\rho_s = 2650$ kg/m^3 the sediment density, and $\rho_w = 1000$ kg/m^3 the water density. The sediment transport rate q_{bk} includes the volume of pores. The nondimensional sediment transport rate is assumed to be a function of the nondimensional bed shear stress, θ_k (Shields, 1936):

$$\theta_k = \frac{C_{fb} u^2}{g R d_k}, \tag{30}$$

where C_{fb} [−] is the skin friction coefficient.

The nondimensional sediment transport rate is computed using a sediment transport relation such as the one proposed by Ashida and Michiue (1971):

$$q_{bk}^* = 17\left(\theta_k - \xi_k \theta_c\right)\left(\sqrt{\theta_k} - \sqrt{\xi_k \theta_c}\right). \tag{31}$$

The parameter ξ_k [−] is the hiding function:

$$\xi_k = \begin{cases} 0.843\left(\dfrac{d_k}{D_m}\right)^{-1} & \text{for } \dfrac{d_k}{D_m} \le 0.4 \\ \left(\dfrac{\log_{10}(19)}{\log_{10}\left(19\dfrac{d_k}{D_m}\right)}\right)^2 & \text{for } \dfrac{d_k}{D_m} > 0.4 \end{cases}, \tag{32}$$

where D_m is a characteristic mean grain size of the sediment mixture. Ashida and Michiue (1971) propose $\theta_c = 0.05$.

Under degradational conditions we assume that the volume fraction content of sediment at the interface between the active layer and the substrate is equal to the sediment in the top part of the substrate. Under aggradational conditions the sediment in the active layer is assumed to be transferred to the substrate (Hirano, 1971):

$$f_k^I = \begin{cases} f_{sk}(z = \eta - L_a) & \text{if } \dfrac{\partial(\eta - L_a)}{\partial t} < 0 \\ F_{ak} & \text{if } \dfrac{\partial(\eta - L_a)}{\partial t} > 0 \end{cases}. \tag{33}$$

Other formulations include those of Hoey and Ferguson (1994).

A.5. Matrix formulation

In this section we present the matrix-vector form (Eq. (1)) of the active layer model in combination with the unsteady flow equations (Stecca et al., 2014) and assuming steady flow (Chavarrías et al., 2018) as well as the simplified morphodynamic model.

The vector of dependent variables ($\mathbf{Q}_u$), system matrix ($\mathbf{A}_u$), and vector of source terms ($\mathbf{S}_u$) of the fully unsteady system is Stecca et al. (2014):

$$\mathbf{Q}_u = \left[h, q, \eta, \underbrace{[M_{ak}]}_{N-1}\right]^T, \tag{34}$$

$$\mathbf{A}_u = \left[\begin{array}{ccc:c} 0 & 1 & 0 & \mathbb{0} \\ gh - \left(\frac{q}{h}\right)^2 & 2\frac{q}{h} & gh & \mathbb{0} \\ \frac{\partial q_b}{\partial h} & \frac{\partial q_b}{\partial q} & 0 & \left[\frac{\partial q_b}{\partial M_{al}}\right] \\ \hdashline \underbrace{\left[\frac{\partial q_{bk}}{\partial h} - f_k^I \frac{\partial q_b}{\partial h}\right]}_{1} & \underbrace{\left[\frac{\partial q_{bk}}{\partial q} - f_k^I \frac{\partial q_b}{\partial q}\right]}_{1} & \underbrace{\mathbb{0}}_{1} & \underbrace{\left[\frac{\partial q_{bk}}{\partial M_{al}} - f_k^I \frac{\partial q_b}{\partial M_{al}}\right]}_{N-1} \end{array}\right] \begin{matrix} \}1 \\ \}1 \\ \}1 \\ \}N-1 \end{matrix}, \tag{35}$$

$$\mathbf{S}_u = \left[0, -ghS_f, 0, \underbrace{\mathbb{0}}_{N-1}\right]^T. \tag{36}$$

The preconditioning matrix is in this case:

$$\mathbf{M}_u = \left[\begin{array}{ccc:c} 1 & 0 & 0 & \\ 0 & 1 & 0 & \mathbb{0} \\ 0 & 0 & \beta & \\ \hdashline & & & \beta\alpha_1 \\ & \mathbb{0} & & \ddots \\ & & & \beta\alpha_{N-1} \end{array}\right]. \tag{37}$$

Assuming steady flow, the vector of dependent variables ($\mathbf{Q}_s$), system matrix ($\mathbf{A}_s$), and vector of source term ($\mathbf{S}_s$) are equal to Chavarrías et al. (2018):

$$\mathbf{Q}_s = \left[\eta, \underbrace{[M_{ak}]}_{N-1}\right]^T, \tag{38}$$

$$\mathbf{A}_s = \left[\begin{array}{c:c} -\frac{1}{1-Fr^2}\frac{\partial q_b}{\partial h} & \left[\frac{\partial q_b}{\partial M_{al}}\right] \\ \hdashline \underbrace{\left[-\frac{1}{1-Fr^2}\left(\frac{\partial q_{bk}}{\partial h} - f_k^I \frac{\partial q_b}{\partial h}\right)\right]}_{1} & \underbrace{\left[\frac{\partial q_{bk}}{\partial M_{al}} - f_k^I \frac{\partial q_b}{\partial M_{al}}\right]}_{N-1} \end{array}\right] \begin{matrix} \}1 \\ \}N-1 \end{matrix}, \tag{39}$$

$$\mathbf{S}_s = \left[\frac{S_f}{1-Fr^2}\frac{\partial q_b}{\partial h}, \underbrace{\left[\frac{S_f}{1-Fr^2}\left(\frac{\partial q_{bk}}{\partial h} - f_k^I \frac{\partial q_b}{\partial h}\right)\right]}_{N-1}\right]^T. \tag{40}$$

The preconditioning matrix assuming steady flow is:

$$\mathbf{M}_s = \beta\left[\begin{array}{c:c} 1 & \mathbb{0} \\ \hdashline & \alpha_1 \\ \mathbb{0} & \ddots \\ & \alpha_{N-1} \end{array}\right]. \tag{41}$$

The nondimensional approximated bed and sorting celerities are (Chavarrías et al., 2018; De Vries, 1965):

$$\lambda_b = \frac{\psi}{1 - Fr^2}, \tag{42}$$

$$\lambda_{s1} = \chi_1 \mu_{1,1}, \tag{43}$$

where the parameters are (Chavarrías et al., 2018; Stecca et al., 2014):

$$\psi = \frac{\partial q_b}{\partial q}, \tag{44}$$

$$\gamma_k = c_k - f_k^I, \tag{45}$$

$$c_k = \frac{1}{\psi}\frac{\partial q_{bk}}{\partial q}, \tag{46}$$

$$\chi_l = \frac{1}{u}\frac{\partial q_b}{\partial M_{al}}, \tag{47}$$

$$\mu_{l,k} = d_{l,k} - f_k^I, \tag{48}$$

$$d_{l,k} = \frac{1}{u\chi_l}\frac{\partial q_{bk}}{\partial M_{al}}. \tag{49}$$

In the simplified morphodynamic model (Section A.3), the vector of dependent variables ($\mathbf{Q}_m$), system matrix ($\mathbf{A}_m$), and vector of source term ($\mathbf{S}_m$) are:

$$\mathbf{Q}_m = [\eta, D_{ma}]^\intercal, \tag{50}$$

$$\mathbf{A}_m = u\begin{bmatrix} -\frac{1}{1-\mathrm{Fr}^2}\frac{\partial q_b}{\partial h} & \frac{\partial q_b}{\partial D_{ma}} \\ \frac{1}{L_a}\frac{1}{1-\mathrm{Fr}^2}\left(D_m^I\frac{\partial q_b}{\partial h} - \sum_{k=1}^{N} d_k\frac{\partial q_{bk}}{\partial h}\right) & -\frac{1}{L_a}\left(D_m^I\frac{\partial q_b}{\partial D_{ma}} - \sum_{k=1}^{N} d_k\frac{\partial q_{bk}}{\partial D_{ma}}\right) \end{bmatrix}, \tag{51}$$

$$\mathbf{S}_m = \frac{S_f}{1-\mathrm{Fr}^2}\left[\frac{\partial q_b}{\partial h}, \frac{-1}{L_a}\left(D_m^I\frac{\partial q_b}{\partial h} - \sum_{k=1}^{N} d_k\frac{\partial q_{bk}}{\partial h}\right)\right]^\intercal. \tag{52}$$

The preconditioning matrix is:

$$\mathbf{M}_m = \beta\begin{bmatrix} 1 & 0 \\ 0 & \alpha \end{bmatrix}. \tag{53}$$

The parameters are:

$$\lambda_m = \chi_m\mu_m, \tag{54}$$

$$\gamma_m = c_m - f_m^I, \tag{55}$$

$$c_m = \frac{1}{\psi L_a}\sum_{k=1}^{N} d_k\frac{\partial q_{bk}}{\partial q}, \tag{56}$$

$$f_m^I = \frac{D_m^I}{L_a}, \tag{57}$$

$$\chi_m = \frac{1}{u}\frac{\partial q_b}{\partial D_{ma}}, \tag{58}$$

$$\mu_m = d_m - f_m^I, \tag{59}$$

$$d_m = \frac{1}{u\chi_m L_a}\sum_{k=1}^{N} d_k\frac{\partial q_{bk}}{\partial D_{ma}}. \tag{60}$$

Appendix B. Mass conservation of the modified system

Mass conservation of the modified system of equations (Section 3.1) is guaranteed if the sum of the N modified active layer equations is equal to the modified (Exner, 1920) equation. As we already substituted the Exner (1920) equation in the active layer equation, the addition of the N modified active layer equations must yield an identity:

$$\begin{aligned} &\sum_{k=1}^{N}\beta\alpha_k\frac{\partial M_{ak}}{\partial t} + \sum_{k=1}^{N} f_k^I\beta\frac{\partial(\eta - L_a)}{\partial t} + \sum_{k=1}^{N}\frac{\partial q_{bk}}{\partial x} = 0 \Rightarrow \\ &\beta\frac{\partial L_a}{\partial t}\left(\sum_{k=1}^{N}\alpha_k F_{ak} - 1\right) + \beta L_a\sum_{k=1}^{N}\left(\alpha_k\frac{\partial F_{ak}}{\partial t}\right) = 0. \end{aligned} \tag{61}$$

To allow for morphodynamic changes the parameter β must be different than 0. This yields a multiplicity of cumbersome closure relations for α_k relating the temporal change of the active layer thickness to those of the volume fraction contents at the bed surface. We choose to simplify the problem assuming that $\alpha_k = \alpha\ \forall k$ so that we obtain:

$$\beta\frac{\partial L_a}{\partial t}(\alpha - 1) = 0. \tag{62}$$

Given that $\alpha \neq 1$ to recover the well-posedness of the system of equation, the active layer thickness must be constant to conserve mass in the modified system of equations.

Appendix C. Parameters of the numerical simulation of the thought experiment

In this section we provide the details of our numerical simulation of the thought experiment conducted by Ribberink (1987). The thought experiment is based on the laboratory Experiment E8-E9 conducted by Ribberink (1987). The only difference is that in the thought experiment the substrate is finer than in the laboratory experiment.

The domain is 30 m long and it is discretized into 0.01 m long cells. The simulation time is 120 h. The total and skin friction coefficient are equal to 0.0117. The sediment mixture is composed of two sediment sizes equal to 0.78 mm and 1.29 mm. The flow discharge per unit width is constant and equal to 0.0803 m^2/s. The downstream water level is constant and such that initially the bed is in equilibrium. The upstream sediment load is initially equal to 5.64×10^{-6} m^2/s and it is composed of 50% of the fine fraction. During the first 30 h the fraction of fine sediment linearly decreases to 0. The total amount of sediment decreases to 95% of the initial value. The active layer thickness is equal to 0.02 m. The initial volume fraction content of fine sediment in the substrate is 0.6.

It is not fully clear to the authors which sediment transport relation and which parameters Ribberink (1987) used in the simulation of the thought experiment using the two-layer model. We have inferred that he used the relation developed by Meyer-Peter and Müller (1948) with the hiding function by Egiazaroff (1965) with the calibrated parameters $A = 15.85$, $B = 1.5$, and $\theta_c = 0.0307$. The mean grain size is computed arithmetically. We calibrate the ripple factor (a constant multiplying the Shields (1936) stress) such that the bed slope and volume fraction content of fine sediment are as close as possible to the reported values. We obtain that for a ripple factor equal to 0.3169 the bed slope is 1.65×10^{-3} (the same as Ribberink (1987) reported) and the volume fraction content of fine sediment in the active layer is equal to 0.409 (Ribberink, 1987 reported a value equal to 0.43).

Supplementary material

Supplementary material associated with this article can be found, in the online version, at doi:10.1016/j.advwatres.2019.04.001.

References

Abgrall, R., Karni, S., 2009. Two-layer shallow water system: a relaxation approach. SIAM J. Sci. Comput. 31 (3), 1603–1627. https://doi.org/10.1137/06067167X.

Allen, J.R.L., 1970. A quantitative model of grain size and sedimentary structures in lateral deposits. Geol. J. 7 (1), 129–146. https://doi.org/10.1002/gj.3350070108.

Ancey, C., Heyman, J., 2014. A microstructural approach to bed load transport: mean behaviour and fluctuations of particle transport rates. J. Fluid Mech. 744, 129–168. https://doi.org/10.1017/jfm.2014.74.

Ardron, K., 1980. One-dimensional two-fluid equations for horizontal stratified two-phase flow. Int. J. Multiphase Flow 6 (4), 295–304. https://doi.org/10.1016/0301-9322(80)90022-1.

Armanini, A., di Silvio, G., 1988. A one-dimensional model for the transport of a sediment mixture in non-equilibrium conditions. J. Hydraul. Res. 26 (3), 275–292. https://doi.org/10.1080/00221688809499212.

Armi, L., 1986. The hydraulics of two flowing layers with different densities. J. Fluid Mech. 163, 27–58. https://doi.org/10.1017/S0022112086002197.

Ashida, K., Michiue, M., 1971. An investigation of river bed degradation downstream of a dam. In: Proc. of the 14th IAHR World Congress, 29 August–3 Septemeber, Paris, France, 3, pp. 247–255.

Bell, R.G., Sutherland, A.J., 1983. Nonequilibrium bedload transport by steady flows. J. Hydraul. Eng. 109 (3). https://doi.org/10.1061/(ASCE)0733-9429(1983)109:3(351).

Blom, A., 2008. Different approaches to handling vertical and streamwise sorting in modeling river morphodynamics. Water Resour. Res. 44 (3), W03415. https://doi.org/10.1029/2006WR005474.

Blom, A., Arkesteijn, L., Chavarrías, V., Viparelli, E., 2017. The equilibrium alluvial river under variable flow and its channel-forming discharge. J. Geophys. Res., Earth Surface 122 (10), 1924–1948. https://doi.org/10.1002/2017JF004213.

Blom, A., Chavarrías, V., Ferguson, R.I., Viparelli, E., 2017. Advance, retreat, and halt of abrupt gravel-sand transitions in alluvial rivers. Geophys. Res. Lett. 44 (19), 9751–9760. https://doi.org/10.1002/2017GL074231.

Blom, A., Parker, G., 2004. Vertical sorting and the morphodynamics of bed-form dominated rivers: a modeling framework. J. Geophys. Res. Earth Surface 109 (F2), F02007. https://doi.org/10.1029/2003JF000069.

Blom, A., Parker, G., Ribberink, J.S., de Vriend, H.J., 2006. Vertical sorting and the morphodynamics of bed-form-dominated rivers: an equilibrium sorting model. J. Geophys. Res. Earth Surface 111 (F1), F01006. https://doi.org/10.1029/2004JF000175.
Blom, A., Ribberink, J.S., Parker, G., 2008. Vertical sorting and the morphodynamics of bed form-dominated rivers: a sorting evolution model. J. Geophys. Res. Earth Surface 113 (F1), F01019. https://doi.org/10.1029/2006JF000618.
Blom, A., Ribberink, J.S., de Vriend, H.J., 2003. Vertical sorting in bed forms: flume experiments with a natural and a trimodal sediment mixture. Water Resour. Res. 39 (2), 1025. https://doi.org/10.1029/2001WR001088.
Blom, A., Viparelli, E., Chavarrías, V., 2016. The graded alluvial river: profile concavity and downstream fining. Geophys. Res. Lett. 43 (12), 6285–6293. https://doi.org/10.1002/2016GL068898.
Cao, Z., Carling, P.A., 2002. Mathematical modelling of alluvial rivers: reality and myth. Part 1: general review. Proc. Inst. Civil Eng. Water Maritime Eng. 154 (3), 207–219.
Cao, Z., Carling, P.A., 2002. Mathematical modelling of alluvial rivers: reality and myth. Part 2: special issues. Proc. Inst. Civil Eng. Water Maritime Eng. 154 (4), 297–307.
Cao, Z., Day, R., Egashira, S., 2002. Coupled and decoupled numerical modeling of flow and morphological evolution in alluvial rivers. J. Hydraul. Eng. 128 (3), 306–321. https://doi.org/10.1061/(ASCE)0733-9429(2002)128:3(306).
Carling, P.A., 1999. Subaqueous gravel dunes. J. Sediment. Res. 69 (3), 534–545. https://doi.org/10.2110/jsr.69.534.
Carling, P.A., Richardson, K., Ikeda, H., 2005. A flume experiment on the development of subaqueous fine-gravel dunes from a lower-stage plane bed. J. Geophys. Res., Earth Surface 110 (F4), F04S05. https://doi.org/10.1029/2004JF000205.
Carraro, F., Vanzo, D., Caleffi, V., Valiani, A., Siviglia, A., 2018. Mathematical study of linear morphodynamic acceleration and derivation of the MASSPEED approach. Adv. Water Resour. 117, 40–52. https://doi.org/10.1016/j.advwatres.2018.05.002.
Castro Díaz, M.J., Fernández Nieto, E.D., González Vida, J.M., Parés Madroñal, C., 2011. Numerical treatment of the loss of hyperbolicity of the two-layer shallow-water system. J. Sci. Comput. 48 (1-3), 16–40. https://doi.org/10.1007/s10915-010-9427-5.
Chavarrías, V., Stecca, G., Blom, A., 2018. Ill-posedness in modelling mixed-sediment river morphodynamics. Adv. Water Resour. 114, 219–235. https://doi.org/10.1016/j.advwatres.2018.02.011.
Chen, S.-C., Peng, S.-H., 2006. Two-dimensional numerical model of two-layer shallow water equations for confluence simulation. Adv. Water Resour. 29 (11), 1608–1617. https://doi.org/10.1016/j.advwatres.2005.12.001.
Chen, S.-C., Peng, S.-H., Capart, H., 2007. Two-layer shallow water computation of mud flow intrusions into quiescent water. J. Hydraul. Res. 45 (1), 13–25. https://doi.org/10.1080/00221686.2007.9521739.
Choi, Y.-H., Merkle, C., 1993. The application of preconditioning in viscous flows. J. Comput. Phys. 105 (2), 207–223. https://doi.org/10.1006/jcph.1993.1069.
Chorin, A.J., 1967. A numerical method for solving incompressible viscous flow problems. J. Comput. Phys. 2 (1), 12–26. https://doi.org/10.1016/0021-9991(67)90037-X.
Colombini, M., Stocchino, A., 2005. Coupling or decoupling bed and flow dynamics: fast and slow sediment waves at high froude numbers. Phys. Fluids 17 (3), 036602. https://doi.org/10.1063/1.1848731.
Cordier, S., Le, M., de Luna, T.M., 2011. Bedload transport in shallow water models: why splitting (may) fail, how hyperbolicity (can) help. Adv. Water Resour. 34 (8), 980–989. https://doi.org/10.1016/j.advwatres.2011.05.002.
Courant, R., Friedrichs, K., Lewy, H., 1928. Über die partiellen Differenzengleichungen der mathematischen Physik. Mathematische Annalen 100, 32–74 (in German).
Courant, R., Hilbert, D., 1989. Methods of Mathematical Physics, Volume 2: Differential Equations. John Wiley & Sons, New York, NY, United States.
Dietrich, W.E., Kirchner, J.W., Ikeda, H., Iseya, F., 1989. Sediment supply and the development of the coarse surface layer in gravel-bedded rivers. Nature 340, 215–217. https://doi.org/10.1038/340215a0.
Drew, D., Cheng, L., Lahey, R., 1979. The analysis of virtual mass effects in two-phase flow. Int. J. Multiphase Flow 5 (4), 233–242. https://doi.org/10.1016/0301-9322(79)90023-5.
Egashira, S., Ashida, K., 1992. Unified View of the Mechanics of Debris Flow and Bed-load. In: Shen, H.H., Satake, M., Mehrabadi, M., Chang, C.S., Campbell, C.S. (Eds.), Advances in Micromechanics of Granular Materials. In: Studies in Applied Mechanics, 31. Elsevier, Amsterdam, the Netherlands, pp. 391–400. https://doi.org/10.1016/B978-0-444-89213-3.50046-8.
Egiazaroff, I.V., 1965. Calculation of nonuniform sediment concentrations. J. Hydraulics Div. 91 (4), 225–247.
Einstein, H.A., 1950. The bed-load function for sediment transportation in open channel flows. Tech. Bull. 1026. US Department of Agriculture, Soil Conservation Service, Washington, DC, United States.
Engelund, F., Hansen, E., 1967. Monograph on sediment transport in alluvial streams. Tech. Rep.. Hydraulics Laboratory, Technical University of Denmark, Copenhagen, Denmark.
Exner, F.M., 1920. Zur Physik der Dünen. Akad. Wiss. Wien Math. Naturwiss 129 (2a), 929–952 (in German).
Feng, J., Merkle, C., 1990. Evaluation of preconditioning methods for time-marching systems. Tech. Rep. 90-0016. AIAA, Washington, DC, United States. https://doi.org/10.2514/6.1990-16.
Fernández Nieto, E.D., 2003. Aproximación numérica de leyes de conservación hiperbólicas no homogéneas. Aplicación a las ecuaciones de aguas someras.. University of Sevilla, Sevilla, Spain Ph.D. thesis (in Spanish).
Furbish, D.J., Haff, P.K., Roseberry, J.C., Schmeeckle, M.W., 2012. A probabilistic description of the bed load sediment flux: 1. theory. J. Geophys. Res. Earth Surface 117 (F3), F03031. https://doi.org/10.1029/2012JF002352.
Garegnani, G., Rosatti, G., Bonaventura, L., 2011. Free surface flows over mobile bed: mathematical analysis and numerical modeling of coupled and decoupled approaches. Commun. Appl. Ind. Math. 2 (1). https://doi.org/10.1685/journal.caim.371.
Garegnani, G., Rosatti, G., Bonaventura, L., 2013. On the range of validity of the Exner-based models for mobile-bed river flow simulations. J. Hydraul. Res. 51 (4), 380–391. https://doi.org/10.1080/00221686.2013.791647.
Godfrey, A.G., Walters, R.W., van Leer, B., 1993. Preconditioning for the Navier–Stokes equations with finite-rate chemistry. Tech. Rep. 1993-535. AIAA, Washington, DC, United States.
Grabowski, W.J., Berger, S.A., 1976. Solutions of the Navier–Stokes equations for vortex breakdown. J. Fluid Mech. 75 (3), 525–544. https://doi.org/10.1017/S0022112076000360.
Gray, J.M.N.T., Ancey, C., 2011. Multi-component particle-size segregation in shallow granular avalanches. J. Fluid Mech. 678, 535–588. https://doi.org/10.1017/jfm.2011.138.
Greco, M., Iervolino, M., Leopardi, A., Vacca, A., 2012. A two-phase model for fast geomorphic shallow flows. Int. J. Sediment Res. 27 (4), 409–425. https://doi.org/10.1016/S1001-6279(13)60001-3.
Greco, M., Iervolino, M., Vacca, A., 2008. Boundary conditions in a two-layer geomorphological model: application to a hydraulic jump over a mobile bed. J. Hydraul. Res. 46 (6), 856–860. https://doi.org/10.1080/00221686.2008.9521933.
Guo, J., 2015. Sidewall and non-uniformity corrections for flume experiments. J. Hydraul. Res. 53 (2), 218–229. https://doi.org/10.1080/00221686.2014.971449.
Hadamard, J.S., 1923. Lectures on Cauchy's Problem in Linear Partial Differential Equations. Yale University Press, New Haven, CT, United States.
Haque, M.I., Mahmood, K., 1983. Analytical determination of form friction factor. J. Hydraul. Eng. 109 (4), 590–610. https://doi.org/10.1061/(ASCE)0733-9429(1983)109:4(590).
Harlow, F.H., Amsden, A.A., 1975. Numerical calculation of multiphase fluid flow. J. Comput. Phys. 17 (1), 19–52. https://doi.org/10.1016/0021-9991(75)90061-3.
Harten, A., Lax, P.D., van Leer, B., 1983. On upstream differencing and Godunov-type schemes for hyperbolic conservation laws. SIAM Rev. 25 (1), 35–61. https://doi.org/10.1137/1025002.
von Helmholtz, H., 1868. Über discontinuierliche Flüssigkeits-Bewegungen. Monatsberichte der Königlichen Preussische Akademie der Wissenschaften zu Berlin 23, 215–228 (in German).
Hirano, M., 1971. River bed degradation with armoring. Proc. Jpn. Soc. Civ. Eng. 195, 55–65. https://doi.org/10.2208/jscej1969.1971.195_55.
Hoey, T.B., Ferguson, R.I., 1994. Numerical simulation of downstream fining by selective transport in gravel bed rivers: model development and illustration. Water Resour. Res. 30 (7), 2251–2260. https://doi.org/10.1029/94WR00556.
Isaacson, E., Temple, B., 1992. Nonlinear resonance in systems of conservation laws. SIAM J. Appl. Math. 52 (5), 1260–1278. https://doi.org/10.1137/0152073.
Ivrii, V.Y., Petkov, V.M., 1974. Necessary conditions for the Cauchy problem for non-strictly hyperbolic equations to be well-posed. Russ. Math. Surv. 29 (5), 1–70.
Johnson, J.W., 1942. The importance of considering sidewall friction in bed-load investigations. Civil Eng. 12, 329–332.
Joseph, D., Saut, J., 1990. Short-wave instabilities and ill-posed initial-value problems. Theor. Comput. Fluid Mech. 1 (4), 191–227. https://doi.org/10.1007/BF00418002.
Kabanikhin, S.I., 2008. Definitions and examples of inverse and ill-posed problems. J. Inv. Ill-Posed Problems 16, 317–357. https://doi.org/10.1515/JIIP.2008.019.
Kelvin, W.T., 1871. Hydrokinetic solutions and observations. Philos. Mag. 42 (281), 362–377. https://doi.org/10.1080/14786447108640585.
Kumbaro, A., Ndjinga, M., 2011. Influence of interfacial pressure term on the hyperbolicity of a general multifluid model. J. Comput. Multiphase Flows 3 (3), 177–195. https://doi.org/10.1260/1757-482X.3.3.177.
Lanzoni, S., Siviglia, A., Frascati, A., Seminara, G., 2006. Long waves in erodible channels and morphodynamic influence. Water Resour. Res. 42 (6). https://doi.org/10.1029/2006WR004916.
Latteux, B., 1995. Techniques for long-term morphological simulation under tidal action. Mar. Geol. 126 (126), 129–141. https://doi.org/10.1016/0025-3227(95)00069-B.
Lawrence, G.A., 1990. On the hydraulics of Boussinesq and non-Boussinesq two-layer flows. J. Fluid Mech. 215, 457–480. https://doi.org/10.1017/S0022112090002713.
Lax, P.D., 1957. Asymptotic solutions of oscillatory initial value problems. Duke Math. J. 24 (4), 627–646. https://doi.org/10.1215/S0012-7094-57-02471-7.
Lax, P.D., 1958. Differential equations, difference equations and matrix theory. Commun. Pure Appl. Math. 11 (2), 175–194. https://doi.org/10.1002/cpa.3160110203.
Lax, P.D., 1980. On the notion of hyperbolicity. Commun. Pure Appl. Math. 33, 395–397.
van Leer, B., Lee, W.-T., Roe, P.L., 1991. Characteristic time-stepping or local preconditioning of the Euler equations. Tech. Rep. 1991-1552. AIAA, Washington, DC, United States.
Lesser, G., Roelvink, J., van Kester, J., Stelling, G., 2004. Development and validation of a three-dimensional morphological model. Coastal Eng. 51, 883–915. https://doi.org/10.1016/j.coastaleng.2004.07.014.
Liska, R., Margolin, L., Wendroff, B., 1995. Nonhydrostatic two-layer models of incompressible flow. Comput. Math. Appl. 29 (9), 25–37. https://doi.org/10.1016/0898-1221(95)00035-W.
Liu, T.-P., 1987. Nonlinear resonance for quasilinear hyperbolic equation. J. Math. Phys. 28 (11), 2593–2602. https://doi.org/10.1063/1.527751.
Long, R.R., 1956. Long waves in a two-fluid system. J. Meteor. 13 (1), 70–74. https://doi.org/10.1175/1520-0469(1956)013<0070:LWIATF>2.0.CO;2.
Love, E., Rider, W., 2013. On the convergence of finite difference methods for PDE under temporal refinement. Comput. Math. Appl. 66 (1), 33–40. https://doi.org/10.1016/j.camwa.2013.04.019.
Luu, X.L., Egashira, S., Takebayashi, H., 2006. A new treatment of the exchange layer thickness to evaluate sediment sorting and armoring. J. Appl. Mech. 9, 1025–1030. https://doi.org/10.2208/journalam.9.1025.
Luu, X.L., Takebayashi, H., Egashira, S., 2004. Characteristics of sediment sorting predicted by two different exchange layer models. Jap. Soc. Fluid Mech. A225, 248–249.

Lyczkowski, R.W., Gidaspow, D., Solbrig, C.W., Hughes, E.D., 1978. Characteristics and stability analyses of transient one-dimensional two-phase flow equations and their finite difference approximations. Nucl. Sci. Eng. 66 (3), 378–396. https://doi.org/10.13182/NSE78-4.

Lyn, D.A., 1987. Unsteady sediment transport modeling. J. Hydraul. Eng. 113 (1), 1–15. https://doi.org/10.1061/(ASCE)0733-9429(1987)113:1(1).

Lyn, D.A., Altinakar, M., 2002. St. Venant–Exner equations for near-critical and transcritical flows. J. Hydraul. Eng. 128 (6), 579–587. https://doi.org/10.1061/(ASCE)0733-9429(2002)128:6(579).

Lyn, D.A., Goodwin, P., 1987. Stability of a general Preissmann scheme. J. Hydraul. Eng. 113 (1), 16–28. https://doi.org/10.1061/(ASCE)0733-9429(1987)113:1(16).

Meyer-Peter, E., Müller, R., 1948. Formulas for bed-load transport. In: Proc. 2nd IAHR World Congress, 6–9 June, Stockholm, Sweden, pp. 39–64.

Mizohata, S., 1961. Some remarks on the Cauchy problem. J. Math. Kyoto Univ. 1 (1), 109–127. https://doi.org/10.1215/kjm/1250525109.

Morris, P.H., Williams, D.J., 1996. Relative celerities of mobile bed flows with finite solids concentrations. J. Hydraul. Eng. 122. https://doi.org/10.1061/(ASCE)0733-9429(1996)122:6(311).

Murray, J.D., 1965. On the mathematics of fluidization. Part 1. fundamental equations and wave propagation. J. Fluid Mech. 21 (3), 465–493. https://doi.org/10.1017/S0022112065000277.

Orrú, C., Blom, A., Chavarrías, V., Ferrara, V., Stecca, G., 2016. A new technique for measuring the bed surface texture during flow and application to a degradational sand-gravel laboratory experiment. Water Resour. Res. 52, 7005–7022. https://doi.org/10.1002/2016WR018938.

Orrú, C., Blom, A., Uijttewaal, W.S.J., 2016. Armor breakup and reformation in a degradational laboratory experiment. Earth Surf. Dyn. 4 (2), 461–470. https://doi.org/10.5194/esurf-4-461-2016.

Paola, C., Voller, V.R., 2005. A generalized Exner equation for sediment mass balance. J. Geophys. Res., Earth Surface 110 (F4), F04014. https://doi.org/10.1029/2004JF000274.

Parker, G., Klingeman, P.C., 1982. On why gravel bed streams are paved. Water Resour. Res. 18 (5), 1409–1423. https://doi.org/10.1029/WR018i005p01409.

Parker, G., Paola, C., Leclair, S., 2000. Probabilistic Exner sediment continuity equation for mixtures with no active layer. J. Hydraul. Eng. 126 (11), 818–826. https://doi.org/10.1061/(ASCE)0733-9429(2000)126:11(818).

Pelanti, M., Bouchut, F., Mangeney, A., 2008. A Roe-type scheme for two-phase shallow granular flows over variable topography. ESAIM: Math. Modell. Numer. Anal. 42 (5), 851–885. https://doi.org/10.1051/m2an:2008029.

Phillips, B.C., Sutherland, A.J., 1989. Spatial lag effects in bed load sediment transport. J. Hydraul. Res. 27 (1), 115–133. https://doi.org/10.1080/00221689009499247.

Phillips, B.C., Sutherland, A.J., 1990. Temporal lag effect in bed load sediment transport. J. Hydraul. Res. 28 (1), 5–23. https://doi.org/10.1080/00221689009499144.

Plows, W.H., 1968. Some numerical results for two-dimensional steady laminar Bénard convection. Phys. Fluids 11 (8), 1593–1599. https://doi.org/10.1063/1.1692166.

Ramshaw, J.D., Trapp, J.A., 1978. Characteristics, stability, and short-wavelength phenomena in two-phase flow equation systems. Nucl. Sci. Eng. 66 (1), 93–102. https://doi.org/10.13182/NSE78-A15191.

Ranasinghe, R., Swinkels, C., Luijendijk, A., Roelvink, D., Bosboom, J., Stive, M., Walstra, D., 2011. Morphodynamic upscaling with the MORFAC approach: Dependencies and sensitivities. Coastal Eng. 58 (8), 806–811. https://doi.org/10.1016/j.coastaleng.2011.03.010.

Recking, A., Frey, P., Paquier, A., Belleudy, P., 2009. An experimental investigation of mechanisms involved in bed load sheet production and migration. J. Geophys. Res. Earth Surface 114 (F3), F03010. https://doi.org/10.1029/2008JF000990.

Ribberink, J.S., 1987. Mathematical modelling of one-dimensional morphological changes in rivers with non-uniform sediment. Delft University of Technology, Delft, the Netherlands Ph.D. thesis.

Roelvink, J., 2006. Coastal morphodynamic evolution techniques. Coastal Eng. 53 (2–3), 277–287. https://doi.org/10.1016/j.coastaleng.2005.10.015.

Roy, C.J., 2005. Review of code and solution verification procedures for computational simulation. J. Comput. Phys. 205 (1), 131–156. https://doi.org/10.1016/j.jcp.2004.10.036.

Saint-Venant, A.J.C.B., 1871. Théorie du mouvement non permanent des eaux, avec application aux crues des rivières et à l'introduction des marées dans leur lit. Comptes Rendus des séances de l'Académie des Sciences 73, 237–240 (in French).

Sarno, L., Carravetta, A., Martino, R., Papa, M., Tai, Y.-C., 2017. Some considerations on numerical schemes for treating hyperbolicity issues in two-layer models. Adv. Water Resour. 100 (Supplement C), 183–198. https://doi.org/10.1016/j.advwatres.2016.12.014.

Savary, C., Zech, Y., 2007. Boundary conditions in a two-layer geomorphological model. application to a hydraulic jump over a mobile bed. J. Hydraul. Res. 45 (3), 316–332. https://doi.org/10.1080/00221686.2007.9521766.

Seminara, G., Colombini, M., Parker, G., 1996. Nearly pure sorting waves and formation of bedload sheets. J. Fluid Mech. 312, 253–278. https://doi.org/10.1017/S0022112096001991.

Shields, A., 1936. Anwendung der Ähnlichkeitsmechanik und Turbulenzforschung auf die Geschiebebewegung. Versuchsanstalt für Wasserbau und Schiffbau, 26, Berlin, Germany Ph.D. thesis (in German).

Sieben, A., 1994. Notes on the mathematical modelling of alluvial mountain rivers with graded sediment. Tech. Rep. 94–3. Faculty of Civil Engineering and Geosciences, Delft University of Technology, Delft, the Netherlands.

Sieben, J., 1997. Modelling of hydraulics and morphology in mountain rivers. Delft University of Technology, Delft, the Netherlands Ph.D. thesis.

Sieben, J., 1999. A theoretical analysis of discontinuous flow with mobile bed. J. Hydraul. Res. 37 (2), 199–212. https://doi.org/10.1080/00221689909498306.

Siviglia, A., Stecca, G., Blom, A., 2017. Modeling of Mixed-sediment Morphodynamics in Gravel Bed rivers Using the Active Layer Approach: Insights from Mathematical and Numerical Analysis. In: Tsutsumi, D., Laronne, J. (Eds.), Gravel-Bed Rivers: Process and Disasters. Wiley-Blackwell, Hoboken, NJ, United States, pp. 703–728. https://doi.org/10.1002/9781118971437.ch26. chap. 26.

Soh, W.Y., Berger, S.A., 1984. Laminar entrance flow in a curved pipe. J. Fluid Mech. 148, 109–135. https://doi.org/10.1017/S0022112084002275.

Spinewine, B., Guinot, V., Soares Frazão, S., Zech, Y., 2011. Solution properties and approximate Riemann solvers for two-layer shallow flow models. Comput. Fluids 44 (1), 202–220. https://doi.org/10.1016/j.compfluid.2011.01.001.

Stecca, G., Siviglia, A., Blom, A., 2014. Mathematical analysis of the Saint-Venant-Hirano model for mixed-sediment morphodynamics. Water Resour. Res. 50, 7563–7589. https://doi.org/10.1002/2014WR015251.

Stecca, G., Siviglia, A., Blom, A., 2016. An accurate numerical solution to the Saint-Venant-Hirano model for mixed-sediment morphodynamics in rivers. Adv. Water Resour. 93, Part A, 39–61. https://doi.org/10.1016/j.advwatres.2015.05.022.

Sternberg, H., 1875. Untersuchungen über Längen- und Querprofil geschiebeführender Flüsse. Zeitschrift für Bauwesen 25, 483–506 (in German).

Stewart, H.B., 1979. Stability of two-phase flow calculation using two-fluid models. J. Comput. Phys. 33 (2), 259–270. https://doi.org/10.1016/0021-9991(79)90020-2.

Stewart, H.B., Wendroff, B., 1984. Two-phase flow: models and methods. J. Comput. Phys. 56 (3), 363–409. https://doi.org/10.1016/0021-9991(84)90103-7.

Stuhmiller, J., 1977. The influence of interfacial pressure forces on the character of two-phase flow model equations. Int. J. Multiphase Flow 3 (6), 551–560. https://doi.org/10.1016/0301-9322(77)90029-5.

Suzuki, K., 1976. On the propagation of a disturbance in the bed composition of an open channel. Tech. Rep. R 1976/09/L. Laboratory of Fluid Mechanics, Faculty of Civil Engineering and Geosciences, Delft University of Technology, Delft, the Netherlands.

Tiselj, I., Petelin, S., 1997. Modelling of two-phase flow with second-order accurate scheme. J. Comput. Phys. 136 (2), 503–521. https://doi.org/10.1006/jcph.1997.5778.

Toro, E.F., 2001. Shock-capturing Methods for Free-surface Shallow Flows. John Wiley & Sons, Hoboken, NJ, United States.

Toro, E.F., 2009. Riemann Solvers and Numerical Methods for Fluid Dynamics, 3rd edition Springer-Verlag Berlin, Heidelberg, Germany. https://doi.org/10.1007/b79761.

Travis, J.R., Harlow, F.H., Amsden, A.A., 1976. Numerical calculation of two-phase flows. Nucl. Sci. Eng. 61 (1), 1–10. https://doi.org/10.13182/NSE76-A28455.

Turkel, E., 1987. Preconditioned methods for solving the incompressible and low speed compressible equations. J. Comput. Phys. 72 (2), 277–298. https://doi.org/10.1016/0021-9991(87)90084-2.

Turkel, E., 1993. Review of preconditioning methods for fluid dynamics. Appl. Numer. Math. 12 (1), 257–284. https://doi.org/10.1016/0168-9274(93)90122-8.

Turkel, E., 1999. Preconditioning techniques in computational fluid dynamics. Annu. Rev. Fluid Mech. 31 (1), 385–416. https://doi.org/10.1146/annurev.fluid.31.1.385.

Viparelli, E., Moreira, R.R.H., Blom, A., 2017. Modelling Stratigraphy-based GBR Morphodynamics.. In: Tsutsumi, D., Laronne, J. (Eds.), Gravel-Bed Rivers: Process and Disasters. Wiley-Blackwell, Hoboken, NJ, United States, pp. 609–637. https://doi.org/10.1002/9781118971437.ch23. chap. 23.

de Vries, M., 1965. Considerations about non-steady bed load transport in open channels. Tech. Rep. 36. Delft Hydraulics Laboratory, Delft, the Netherlands.

Whiting, P.J., Dietrich, W.E., Leopold, L.B., Drake, T.G., Shreve, R.L., 1988. Bedload sheets in heterogeneous sediment. Geology 16 (2), 105–108. https://doi.org/10.1130/0091-7613(1988)016<0105:BSIHS>2.3.CO;2.

Wong, M., Parker, G., 2006. One-dimensional modeling of bed evolution in a gravel bed river subject to a cycled flood hydrograph. J. Geophys. Res., Earth Surface 111 (F3), F03018. https://doi.org/10.1029/2006JF000478.

Wright, S., Parker, G., 2004. Flow resistance and suspended load in sand-bed rivers: Simplified stratification model. J. Hydraul. Eng. 130 (8), 796–805. https://doi.org/10.1061/(ASCE)0733-9429(2004)130:8(796).

Wu, W., 2007. Computational River Dynamics. Taylor & Francis, London, United Kingdom.

Zanotti, A.L., Méndez, C.G., Nigro, N.M., Storti, M., 2007. A preconditioning mass matrix to avoid the ill-posed two-fluid model. J. Appl. Mech. 74(4), 732–740. https://doi.org/10.1115/1.2711224.